

1-22-1988

## Appearance Potential Spectroscopy of Solid Surfaces

D. R. Chopra

*East Texas State University*

A. R. Chourasia

*East Texas State University*

Follow this and additional works at: <https://digitalcommons.usu.edu/microscopy>



Part of the [Life Sciences Commons](#)

---

### Recommended Citation

Chopra, D. R. and Chourasia, A. R. (1988) "Appearance Potential Spectroscopy of Solid Surfaces," *Scanning Microscopy*. Vol. 2 : No. 2 , Article 7.

Available at: <https://digitalcommons.usu.edu/microscopy/vol2/iss2/7>

This Article is brought to you for free and open access by the Western Dairy Center at DigitalCommons@USU. It has been accepted for inclusion in Scanning Microscopy by an authorized administrator of DigitalCommons@USU. For more information, please contact [digitalcommons@usu.edu](mailto:digitalcommons@usu.edu).



## APPEARANCE POTENTIAL SPECTROSCOPY OF SOLID SURFACES

D. R. Chopra\* and A. R. Chourasia

Department of Physics  
East Texas State University  
Commerce, Texas 75428 USA.

(Received for publication May 17, 1987, and in revised form January 22, 1988)

### Abstract

Among the techniques utilized for the study of unfilled density of states above the Fermi level in a system, appearance potential spectroscopy (APS) has emerged as one of the simplest. Some review papers on APS have appeared in the last decade. Since then APS has been applied to several interesting systems, the studies of which have been limited by other experimental techniques available. This paper reviews some of these applications of APS. We discuss briefly the one-electron theory describing the APS process and outline the basic experimental set-ups used by workers in this field. We then survey some important applications of this technique to simple, as well as, multi-component systems. The results of the applications cited are compared with those from other techniques wherever available. The electronic structure of transition metals, rare earths and their intermetallics as obtained from APS spectra are discussed. The phenomena of adsorption and fine structure which are dependent on the surface sensitivity of APS are also dealt with by including some interesting applications. Finally, we take into account the strengths and limitations of this technique and outline the prospects of this spectroscopy in attaining its importance among the various surface spectroscopies.

**KEY WORDS:** Threshold, Spectroscopy, Appearance, Soft X-ray, Auger, Transition Metals, Rare Earths, Intermetallics, Adsorption, Fine Structure.

\*Address for Correspondence:  
Department of Physics,  
East Texas State University,  
Commerce, Texas 75428. USA.

Phone No.: (214) 886-5484

### Introduction

With the increased influence of surfaces on the functioning of devices in the micro-electronics industry, a host of new tools have been developed in the last decade to analyze the atomic structures of surfaces [95]. Most of these tools (such as Auger electron and X-ray photoelectron spectroscopies) have been devoted to spectroscopic investigation of the electronic density of occupied states in solids. From such studies on the binding energy (BE) of core electrons, in particular, important information on the electronic structure of a material can be obtained. These, in turn, permit determination of the effective charges on the atoms and the polarity of the bonds between atoms of different types in alloys or compounds [6]. Comparatively few experiments have been carried out to measure the density of unoccupied electronic states. Appropriate experimental methods have been discussed by Nagel [65]. Among the techniques used to probe the density of unoccupied electronic states, x-ray absorption (XAS), bremsstrahlung isochromat (BIS), inverse photoemission (IPE), and appearance potential (APS) spectroscopies have proved to be the most promising approaches.

In XAS the incident x-rays traverse through the sample. X-rays of appropriate energy are absorbed by the atoms and, as a result, a core electron is excited to an unoccupied state above the Fermi energy,  $E_F$ . The decrease in the transmitted x-ray intensity is measured. However, in this spectroscopy selection rules are rigorously obeyed and all symmetries must be considered to interpret the spectral features. The schematic diagram, in the one electron approximation, of the X-ray excitation of a core state is shown in fig.1.

In BIS, the sample to be investigated serves as the anode of an x-ray tube. An x-ray spectrometer, tuned to a

fixed quantum energy  $\hbar\omega_0$ , records the bremsstrahlung yield as a function of the accelerating voltage across the tube. Those electrons with initial energy  $E$  with respect to  $E_F$  of the anode, which undergo radiative transitions with emission of a quantum of energy  $\hbar\omega_0$  show up in final states in the conduction band of the sample at an energy  $E - \hbar\omega_0$ .

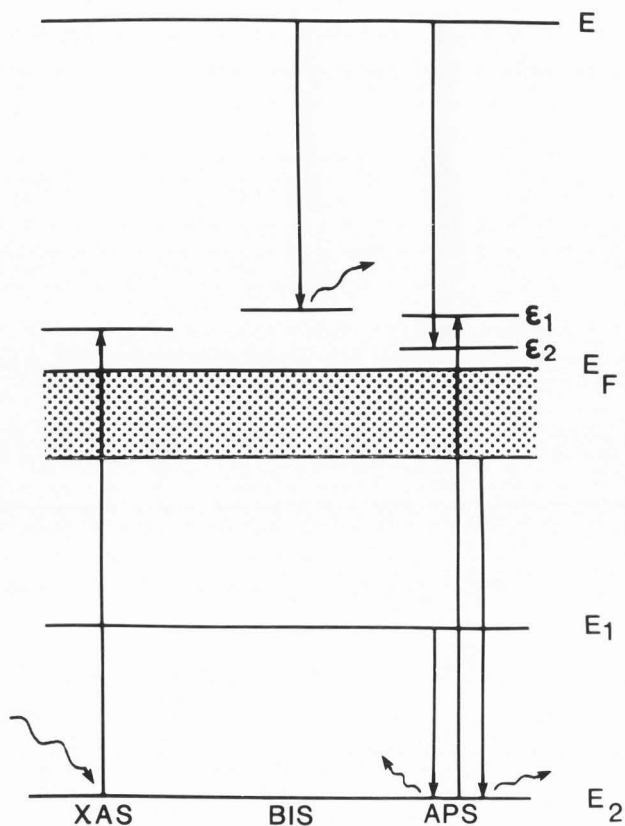


FIGURE 1: Schematic diagram showing electron excitation of a core state in X-ray absorption (left), bremsstrahlung emission (middle) and appearance potential (right) spectroscopies.

Assuming a constant radiative matrix element, the transition probability will be proportional to the density of the final unfilled states. The measured yield will, therefore, directly reflect the density of empty one-electron states. The corresponding schematic diagram is also shown in fig.1. Inverse photoemission (IPE) spectroscopy represents an important and growing area of the present-day surface analysis [28]. Measurements in it are carried out in a manner very similar

to those done with the BIS technique. In this spectroscopy, the energy of incident electrons is no more than a few tens of electron volts. This technique is, therefore, sensitive to the surface region because of the finite path length of low energy electrons. The simple model stated above has been shown to be valid for isochromat results in the X-ray energy range, where the method can be regarded as inverse to XPS [46,54, 61,80,97] and hence the name inverse photoemission.

Appearance potential spectroscopy measures the probability for electronic excitation of a core level as a function of incident electron energy. The experiment consists of a simple triode arrangement. The energy of the incident electrons is gradually increased, and the dependence of the total signal strength on this energy is measured. At certain energies a sudden change (increase or decrease) of the signal is observed, which is connected with the excitation of a given energy level of the sample. The signal is extracted by a potential modulation technique. The corresponding transitions in the one electron approximation are included in fig.1. Because of its experimental and conceptual simplicity and the ability to obtain detailed information from structures superimposed on a large background [67,77,87] APS has received considerable attention. As a tool for chemical analysis it has its merits when compared with other techniques, especially when applied to multiple component alloys [23,98]. APS has also been shown to be sensitive to adsorption phenomena [4,34,68,69]. Chemisorption and oxidation phases can be distinguished [68]. The special advantages of APS over other spectroscopies are that it is a non-dispersive technique and the peaks in the spectrum are specific to a single element. This makes it experimentally simple and allows one to separately examine the states accessible to core electrons of different elements on the same surface. An important aspect of APS is that it reveals a localized density of states because the matrix element governing the core hole production involves the very short range wave function of the initial core electron state. Since electronic excitation does not obey selection rules, APS reveals information regarding the total DOS. As compared to this, XAS measures only specific symmetry characters. As stated above, APS does not require a dispersive analyzer in contrast to other techniques. It thus measures energy rather than momentum. This accounts for the extreme simplicity of the APS spectrometer.

## Appearance Potential Spectroscopy

When the spectra obtained by these techniques are compared, they often give similar results for the same material. Therefore certain features in the spectra can be consistently associated with corresponding structures in the electronic configuration of the substance being studied. The remaining differences are caused by a variety of effects such as transport phenomena and varying transition probabilities, and these must be accounted for before any definitive comparison between theoretical calculations and experimental results is made.

APS, a fairly old technique, was formulated in 1921 [81]. Due to the experimental limitations observed at that time, it was abandoned in 1933. In the 1950's it was briefly revived by Shinoda et al., [85]. Later in the 1970's it was developed as a practical tool for the study of the electronic structure and composition of solid surfaces by Park et al., [75,78]. An excellent historical introduction has been given in Ref. [77].

In APS thermally excited electrons are used as a source of excitation of the core levels of atoms in the surface region. Fukuda et al. [37] have used a field-emission electron source. For electron beams with energy under 2 keV, the short mean free path [82] for inelastic scattering makes this technique surface-sensitive. The excitation of the level can be monitored in several ways: 1) The intensity of the emitted x-rays is measured; the method is called Soft X-ray APS or SXAPS [78], 2) The total current of the secondary electrons is measured; the method is called Auger electron APS or AEAPS [39,47], and 3) The current of the elastically reflected electrons is measured. As a certain number of electrons are scattered inelastically at the threshold energy of core level excitation, they disappear from the measured current, and the method is therefore called Disappearance Potential Spectroscopy or DAPS [50]. In SXAPS and AEAPS techniques an increase of the secondary flux at an excitation threshold is observed. The intensity depends on the fluorescence and Auger yields respectively, which, in turn, depends on the type of electron shell, on the binding energy, and on the atomic environment [5]. These methods give results based on the details of the deexcitation mechanism, whereas, DAPS is free of these complications.

The main information [76] that can be obtained from an APS spectrum can be summarized as follows: 1) The spectral lines provide a simple means for identifying the surface constituents. 2) The threshold of the spectral line corrected for the work function of the electron source and the energy spread of the incident electrons measures the BE of the

corresponding core level. 3) The chemical shifts, in the position of the spectral line, give information about the changes in the chemical bonding. 4) The shape of the peak gives an indirect characterization of the unfilled density of states in the valence band [77] which is also influenced by surface effects [56]. 5) The height of the peak is proportional to the square of the local density of states at the Fermi level provided that the density of states attains a maximum at  $E_F$ . In addition to these the analysis of the 3d transition metals indicates the following characteristics: 6) The width of the positive peak approximates the width of the unfilled portion of the 3d band, and 7) In the absence of the 4sp band, the height of the negative peak should equal the positive peak. The decrease in the negative peak thus measures the contribution of the 4sp states to the 3d band.

In the last decade the APS technique has been reviewed [9,42,77]. Since then many new applications unique to this technique have been reported. The purpose of this paper is, therefore, to review these developments underlying the potential applications of APS to the modern technology.

The paper is organized as follows. In the next section we illustrate the one-electron model governing the APS spectral features. In the "Experimental" section some experimental understanding is given about the different set-ups. The remaining sections are devoted to the applications of APS. In the "Transition Metals" section we discuss the elucidation of the electronic structure of the 3d transition metals. More important in this section is the possibility of deriving density of states directly from the APS spectrum. The "Rare Earths" section deals with the discussion on the rare earths. The one-electron theory explaining satisfactorily the 3d transition metal spectra fails when applied to rare earths. We discuss in this section some of our results on rare earths. In the "Intermetallics" section we take some interesting intermetallics and show how the change in their electronic structure can be studied. The "Adsorption" and "Fine Structure" sections are devoted to the other important applications of APS. The adsorption of gases on 3d transition metals is purely a surface phenomenon which can very well be studied by APS and is discussed in the "Adsorption" section. The unique feature of such a study is that it is possible to distinguish between chemisorbed and oxide phases in the case of oxygen exposure to the metals. In the "Fine Structure"

section is shown the application of the extended appearance potential fine structure (EAPFS) observed in the APS spectra for the determination of geometrical information about surfaces. The analogous bulk technique (extended X-ray absorption fine structure, EXAFS) is not common to all laboratories. EAPFS, due to its experimental simplicity, is a widely available option for fine structure measurements in any surface analysis laboratory. Finally in the "Summary" section we discuss the merits and demerits of APS and look into the diversification of this spectroscopy as a more desirable technique for surface analysis.

### Theoretical Model

In APS the surface of a solid is bombarded with monochromatic electrons

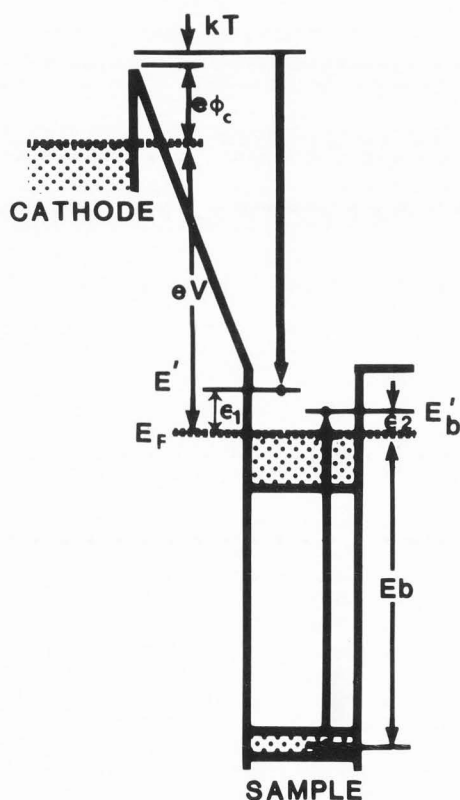


FIGURE 2: Electron excitation in APS. The core electron may scatter into a state  $\epsilon_2 = eV + e\phi_c + kT - \epsilon_1 - E$ . The core hole may subsequently decay by the emission of characteristic X-rays.

having energy (E) in the range 0 to 2000 eV. If the incident electron is captured by a state  $\epsilon_1$  above  $E_F$ , the energy may be conserved by the excitation of a core electron into a state  $\epsilon_2$  as shown in fig.2, and is given by:

$$\epsilon_2 = eV + e\phi_c + kT - \epsilon_1 - E_b \quad (1)$$

where V is the potential applied between a thermionic emitter and the anode,  $e\phi_c$  is the emitter work function, kT is the average thermal energy of the emitted electrons and  $E_b$  is the BE of the core electron relative to  $E_F$ .

The recombination of the core hole may take place radiatively by the emission of a characteristic x-ray photon. This characteristic emission has a distinct threshold given by:

$$E_b = eV + e\phi_c + kT \quad (2)$$

In the case of tungsten filament the work function  $e\phi_c$  is 4.5 eV. The corrections [76] due to the amplitude of the modulating voltage and the thermal energy spread of the incident electrons amount to 0.5 eV. Thus the total correction comes to 5.0 eV. This value needs to be added to the values obtained in the recorder plots so as to make the determination of BE directly. The absolute value of BE can be determined without correction for emitter work function by using a field-emission electron source. This is discussed later in this section.

The total x-ray yield Y(E) contains two contributions,  $Y_B(E)$ , from the bremsstrahlung emission, and  $Y_C(E)$ , from the characteristic x-rays [77,87]:

$$Y(E) = Y_C(E) + Y_B(E) \quad (3)$$

The characteristic x-rays are generated by the radiative decay of the core holes created by the incident electrons. Therefore  $Y_C(E)$  is given by:

$$Y_C(E) = \sum_n P_n \sigma_n(E) \quad (4)$$

The summation is over all states having  $E_b < E$ .  $P_n$  is the probability for the radiative decay of the core state n and is independent of the incident electron energy.  $\sigma_n(E)$ , the excitation cross-section of an electron in the subshell n, represents a function which is zero for  $E < E_b$  and smooth for  $E > E_b$ . It represents the ground state  $\phi$  and excited state  $f(E_0, E)$  with one-electron wave functions, and is given by:

$$\sigma(E) = \int_0^E \phi(E - E_b) f(E, E_b) dE \quad (5)$$

where  $\phi(E - E_b)$  represents the core level Lorentzian function. The function

## Appearance Potential Spectroscopy

$f(E, E_b)$  must take into account both the electron promoted to the Fermi level and the scattered incident electron, and is given by:

$$f(E, E_b) = \int_0^{E-E_b} p_1(\epsilon_1, E) p_2(\epsilon_2, E) N(\epsilon_1) N(\epsilon_2) d\epsilon_2, \quad (6)$$

where  $\epsilon_1 + \epsilon_2 = E - E_b$ . The factors  $p_1(\epsilon_1, E)$  and  $p_2(\epsilon_2, E)$  representing the respective transition probabilities, may depend on selection rules, and are unknown. If these factors are assumed to be independent of  $\epsilon$  and  $E$  over a small range of  $E$  values above the threshold value  $E_b$ , then they can be taken as simply proportional to  $N(\epsilon)$ . Eqn. (6) reduces to:

$$f(E, E_b) = \int_0^{E-E_b} N(E - E_b - \epsilon_2) N(\epsilon_2) d\epsilon_2, \quad (7)$$

which is simply the self-convolution of the density of conduction band states. In APS, the derivative APS(E) of the yield is determined experimentally. Therefore, differentiating eqn. (5) and taking the core level density of states as Dirac delta function, we get:

$$\text{APS}(E) = \frac{d}{dE} \int_0^{E-E_b} N(\epsilon_2) d\epsilon_2 = N(0)N(E - E_b) + \int_0^{E-E_b} N(\epsilon_2) \frac{d}{dE} N(E - E_b - \epsilon_2) d\epsilon_2. \quad (8)$$

At  $E_F$  the first term vanishes. The structure in the APS spectrum is then given by the second term. For a simple step-like density of empty states the derivative  $dN(E - E_b - \epsilon_2)/dE$  can be approximated [9] by  $N_{EF}\delta E$ , where  $N_{EF}$  is the density of states at the threshold and  $\delta E$  is the Dirac delta function. Therefore:

$$\text{APS}(E) = N_{EF} \cdot N(E - E_b). \quad (9)$$

The intensity at the threshold is then given by:

$$\text{APS}(E) = N_{EF}^2 \quad (10)$$

i.e., the height of the structure above the background is proportional to the square of the density of states at  $E_F$ .

APS is very sensitive to DOS at  $E_F$ . Thus elements having low DOS give a weak signal in the spectrum. In fig.3 is shown the schematic representation of the DOS for transition and noble metals and is taken from ref.[72]. The Fermi energy  $E_F$  in the case of transition metals lies in a narrow, partially filled d-band as shown in fig.3a. The one-electron density of states is given by  $N(E)$ . The two-electron density of conduction states  $N_{2c}(E)$  is given by the self-convolution of  $N(E)$

above  $E_F$ . The dotted curve is the derivative of this function and is characterized by a negative dip. For metals having filled d bands the situation is shown in fig.3b. The derivative of  $N_{2c}(E)$  is a step-like function shown dotted in the figure. In actual practice, the APS spectrum looks like the dotted curves but broadened by the core-level lifetime width and the instrument response function.

The instrument response function results primarily from the amplitude of the potential modulation. The threshold peak widths measured at half-maximum must be corrected for this response function in order to draw meaningful conclusions. The corrected widths ( $W_C$ ) can be calculated from:

$$W_C = [ (W_M)^2 - (W_p)^2 ]^{1/2} \quad (11)$$

where  $W_M$  is the measured width of the threshold peak and  $W_p$  is the peak-to-peak modulation voltage applied.

In earlier measurements the BE in an APS spectrum was determined in a simple way by the intersection of the extrapolated projection of the background and positive going low energy slope of the peak. Since the APS yield is proportional to the self-convolution of the density of the final electron states broadened by the finite lifetime of the core hole and by the finite experimental resolution, precise knowledge about BE can be obtained by using deconvolution techniques. Successful deconvolution techniques have been developed by Fukuda et al. [37], Dose et al. [20] and Schulz et al. [84].

As stated earlier, the BE in APS is obtained directly from the recorder plots by applying the correction for the work function of the thermionic electron source. To avoid the uncertainty introduced due to this correction in the BE measurements, Fukuda et al. [37] have used a field-emission electron source. In this the field-emitted electrons tunnel through the potential barrier at the emitter surface. Therefore, no correction for the work function is required. Using such an electron source, absolute  $2p_{3/2}$  core level BEs have been determined for 3d transition metals from their APS spectra corrected for the lifetime broadening of the core state [37].

### Experimental

In SXAPS the total soft x-ray intensity emitted by a sample under electron bombardment is measured as a function of incident electron energy [77]. The schematic of this spectrometer is shown in fig.4. Electrons from a

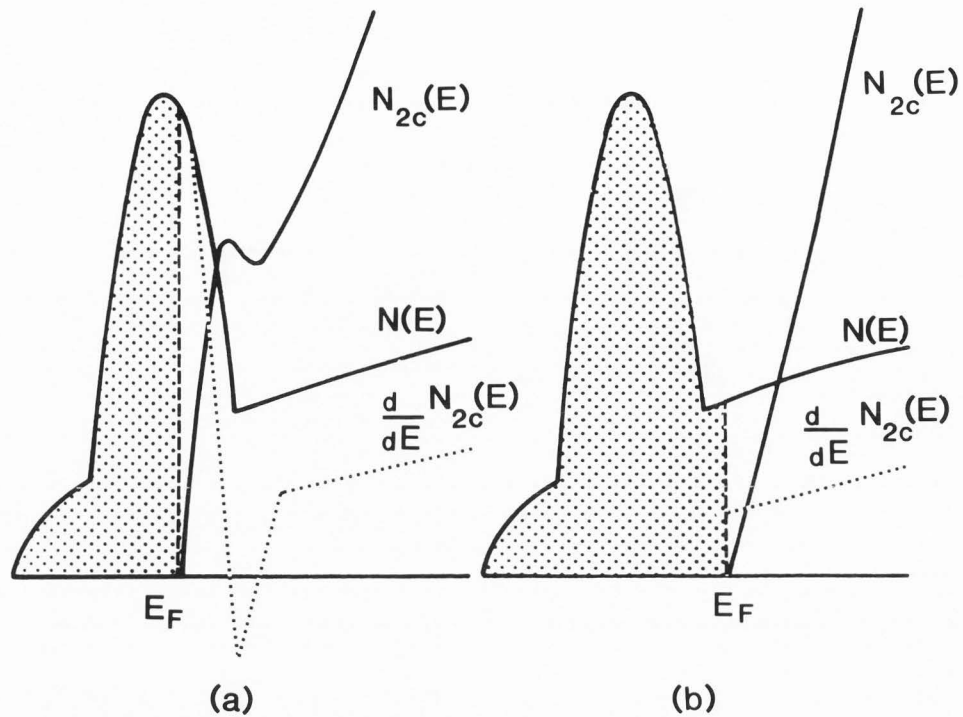


FIGURE 3: Schematic representation of the DOS in APS. (a) Partially filled d band for transition metals.  $N(E)$  is the one-electron DOS. The two electron density of conduction states  $N_{2c}(E)$  is given by the self-convolution of  $N(E)$  above  $E_F$ . The derivative of this function is the dotted curve and is characterized by a sharp peak at  $E_F$  followed by a negative dip. (b) The d band just filled for noble metals. The derivative of  $N_{2c}(E)$  is a step-like function. The figures are reproduced by permission from ref. [72].

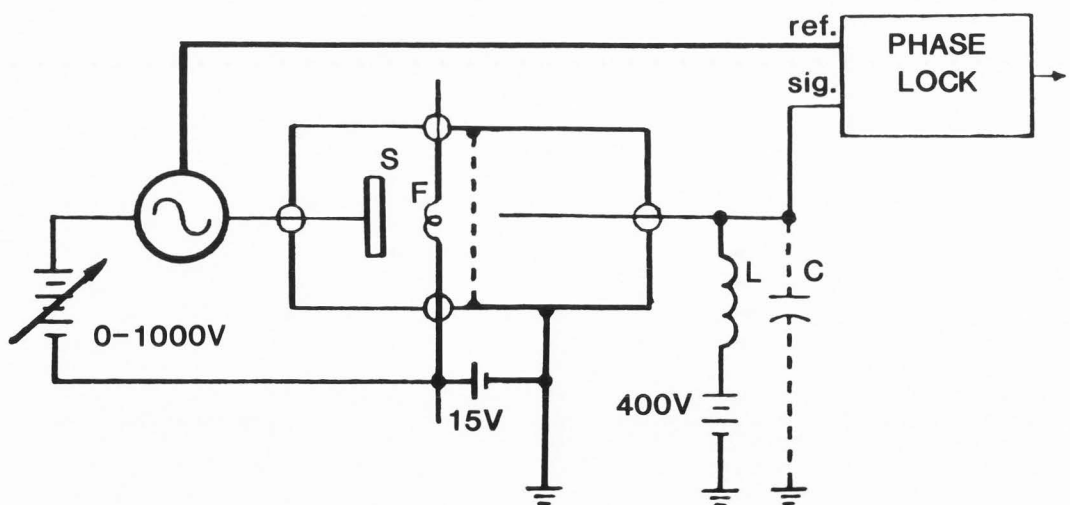
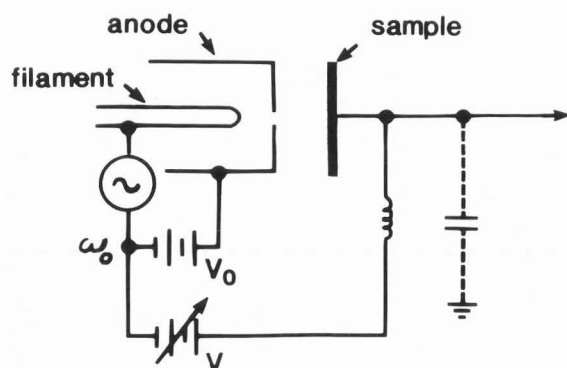


FIGURE 4: Simplified schematic of the soft X-ray appearance potential spectrometer. S is the sample and F is the filament.

## Appearance Potential Spectroscopy

tungsten filament F impinge on the sample S to be studied. A grid electrically separates the filament-target and the detector assemblies. The entire system is enclosed in a stainless steel chamber and is maintained under UHV conditions. X-rays passing through the grid strike the walls of the chamber which act as a photocathode. The resulting photoelectrons are collected on an electrode which is biased at +300 V. The filament is biased positive with respect to the chamber walls in order to prevent the electrons from reaching the collector. The extraction of the signal in the first differential mode is accomplished by the modulation technique. The accelerating voltage is modulated by a small sinusoidal signal. The output is synchronously detected and amplified with the help of a phase-lock amplifier. Details of the experimental technique are available in Refs. [11,77,78].

AEAPS spectrometer is very much similar to the SXAPS except for some minor changes. The spectrometer fabricated in our laboratory [40] consists of a triode arrangement and is shown in fig.5. The anode completely surrounds



**FIGURE 5:** Schematic diagram of Auger electron appearance potential spectrometer. Field-emitted electrons passing through an aperture in the anode impinge on the sample. Signal is extracted by the potential modulation technique.

the filament except for a one mm exit aperture in the top of the anode as shown. The target sample is mounted directly above the aperture. Electrons emitted from the filament are accelerated to the anode by a constant potential. The target is also at a positive potential and is linearly varied by a programmable ramp generator. The anode potential is held at a voltage that is higher than the maximum voltage of the ramp for a certain

core state; therefore the anode serves as a collector of back-scattered electrons. The current in the anode-sample circuit is then:

$$I = I_p - I_s \quad (12)$$

where  $I_p$  is the primary electron current, and  $I_s$  is the secondary electron current. This  $I_s$  arises as a result of the interaction of primary electrons and the sample. Because the anode potential is kept constant, the primary current remains constant. Variations in  $I$  then reflect changes in the secondary current only. An increase in  $I_s$  due to the emission of Auger electrons accompanying the onset of a core level excitation will indicate a sudden decrease in  $I$ . Extraction of this information is accomplished by differentiating the secondary current with respect to the target voltage. This is done by superimposing a small signal in the filament circuit. The secondary current in the anode-sample circuit that varies at this frequency is then synchronously detected with a phase-lock amplifier. Because the secondary electron emission does not exhibit a linear dependence on incident electron energy, it is generally advantageous to make measurements in the second derivative mode.

Single-crystal materials exhibit a complicated AEAPS spectra at low energies [74]. In fact, the APS structure is completely masked by a low energy electron diffraction (LEED) structure. This structure is formed only by elastically scattered electrons. To separate the elastic and inelastic contributions to the APS spectra, Eckertova and Pavluch [29,79] have suggested a use of a 3-grid hemispherical system in a special arrangement. A schematic representation of this system is shown in fig.6. The grid  $G_1$  has the same potential as that of the sample. The grid  $G_2$  operates on a positive potential and collects the backscattered electrons. Some of these electrons strike  $G_2$  while others pass through the space between  $G_2$  and  $G_3$ .  $G_3$  has a negative potential and controls the operation of the spectrometer. There are two modes of operation of the spectrometer: the low energy APS (known as LEAPS) and the high energy APS (known as HEAPS) measurements. The limit between these two modes is determined by the potential of  $G_3$ . By changing this potential the contributions of electrons with different energies can be obtained. The advantages of such a modified spectrometer are that it reduces the effect of the primary current on the spectra and also reduces the non-linearity of the

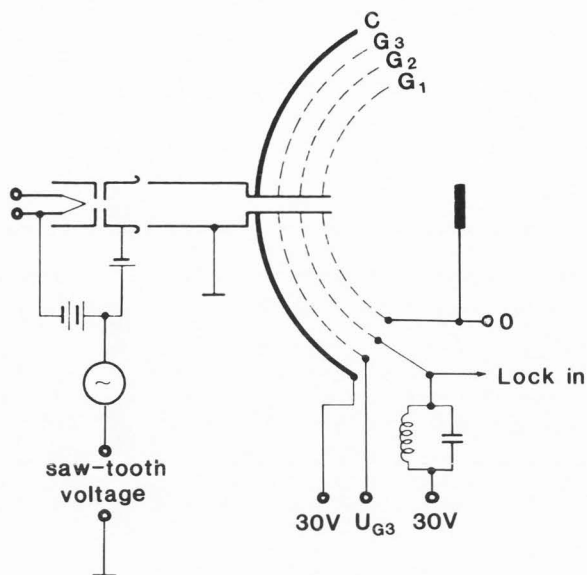


FIGURE 6: Schematic of the LEAPS method. Grid  $G_3$  controls the operation of the spectrometer. The same set-up could be used for DAPS by applying proper voltage to  $G_3$ . The figure is reproduced by permission from ref. [29].

electron gun. With these modifications the signal to background ratio is considerably enhanced, thus facilitating good interpretation of the spectra, especially in the case of single crystals. Due to the smooth background the fine structure appearing on the high energy side of a particular core level spectrum can be easily detected and analyzed to obtain important information. Konishi et al. [51] have also used a similar spectrometer to carry out the AEAPS analyses. The DAPS spectrum can be measured with the same spectrometer shown in fig.6 by changing the potential of the grid  $G_3$ . At a particular potential applied to  $G_3$  the secondary electron current at the threshold decreases. The elastically reflected electrons then constitute the DAPS signal.

The major problem encountered in APS is the signal-to-noise ratio. In the SXAPS a broad-band noise is present due to Bremsstrahlung photons, and this increases steadily with the primary electron energy [96]. In AEAPS, the yield of low energy secondary electrons is not a simple function of the primary electron energy and depends sensitively on the

surface conditions. In DAPS, the back-scattering cross section of the electrons in the solid is low. This makes the total reflection coefficient rather small (of the order of  $10^{-3}$  to  $10^{-2}$ ) which in turn reduces the signal-to-noise ratio. Andersson et al. [2] have designed a low noise SXAPS spectrometer to improve the signal-to-noise ratio. It consists of a silicon surface-barrier diode detector cooled with liquid nitrogen. They have used an Al window to filter out low energy photons. Lee [60] has discussed the signal-to-noise performance of SXAPS spectrometer in the cases of quantum and energy detectors. He found that in the useful electron energy range, the sensitivity of energy detectors is superior to that of quantum detectors using x-ray filter. He suggested the use of an energy detector with unity quantum efficiency and the largest possible collection efficiency in order to achieve maximum sensitivity in SXAPS spectrometer. The sensitivity can further be enhanced by geometrical arrangement of the detector, the electron beam and the sample.

The resolution of the spectrometer depends on several factors, such as the voltage drop across the filament, the thermal energy spread of the incident electron energy and the amplitude of the modulation voltage. Taking such factors into consideration, the resolution in SXAPS can be kept [72] below 0.5 eV, making it the highest resolution core-level spectroscopy available.

### Transition Metals

Core level BE data are used in a number of surface spectroscopies. It is usually assumed that BEs determined by one technique are the same as those determined by others. It has, however, been shown that small but significant differences do exist in BEs measured by different methods [1,35]. Fundamental differences have been found between the BEs measured by APS and x-ray photoelectron spectroscopy (XPS). XPS values have generally appeared to be larger than those measured by APS. This may result from the substantial difference in final states in the two types of spectroscopies [38]. APS normally measures the BE of negative ions whereas XPS values are characteristic of positive ions. Webb and Williams [99] have found close agreement between APS and XPS values for Fe and Ni. They suggested that the core-level widths and surface chemical shifts contribute to the differences between BEs obtained with the two techniques. A series of measurements of the  $L_3$ -shell BEs of six 3d transition metals by XPS, AEAPS, and

## Appearance Potential Spectroscopy

core-level electron energy-loss spectroscopy (EELS) was made with the same specimen materials and the same reference power supplies [32]. This study indicates that BE differences up to about 1.5 eV can occur.

Anderson et al. [1] have made use of a new photoelectron spectroscopy technique to carry out a meaningful comparison of XPS and APS BEs. This technique is called Fermi-level Referenced Electron Spectroscopy for Chemical Analysis (FRESCA). It has the principal advantage of yielding absolute measurements of the energy of photoelectrons. It also eliminates most of the inherent sources of error in XPS and does not require BE standards to relate the measurements to an absolute energy scale. The BEs measured with FRESCA and APS agree very well at lower energies in the case of transition metals. At energies above 600 eV significant differences are observed. Anderson et al. [1] suggest that this effect may be primarily related to the filling of the d-band rather than to the energy of the exciting photoelectrons. In reality there can be different final states and a varying screening response of the solid for each type of excitation. Until these effects are clearly understood, accurate BE data for one spectroscopy should not be assumed to be applicable to other spectroscopies with the same accuracy.

Overall, the BEs of the  $L_2$ ,  $L_3$  core levels of transition metals derived from APS spectra are in all cases lower than the literature values [6]. Dev and Brinkman [18] correlated these surface chemical shifts to the reduced coordination of the surface atoms resulting from the low penetration depths of incident electrons. It is important to note that the measurement of energy level differences is simpler and more precise because these are not affected by the distribution of valence electrons. The observed APS spectral peaks show excellent agreement with the  $L_3$ - $L_2$  spin orbit intervals for the 3d transition elements.

On the basis of a one-electron model, it is expected that the APS spectrum of a given core level of a 3d transition metal will exhibit a positive threshold peak whose width is determined by the width of an unoccupied 3d band, followed by a negative-going peak. In the absence of overlap between 3d and 4sp bands, the negative peak would equal the positive peak. The size of the negative peak therefore reflects the relative contribution of the 4sp states. The systematic study [76] of the  $L_{2,3}$  levels APS spectra shows a progressive decrease in the width of the 3d bands and in the size of the negative peak with Z. These measured widths after correction for the

lifetime broadening of  $L_3$  level are in excellent agreement with Snow and Waber's [88] calculations and clearly indicate that 3d transition series elements follow a rigid-band model. On the basis of the rigid-band model, it is anticipated for the 2p spectra of Cu, for which the 3d band is full, to display steps at the  $L_3$  and  $L_2$  thresholds instead of the positive peak which is characteristic of the 3d series elements. The predictions of the theory are borne out by the experiment [76], and Cu indeed is void of any distinctive positive peak, as expected.

Ertl and Wandelt [33] have studied the Ni/Cu alloys by SXAPS to determine the variation with alloy composition of the densities of states at  $E_F$ . According to the rigid band model the d states of Ni should be completely filled at higher Cu concentrations. Consequently, no Ni  $L_{2,3}$  peaks should show up in the alloys with higher Cu concentration. However, pronounced peaks were observed in the Ni  $L_{2,3}$  region even in alloys with more than 55 % Cu. These peaks are caused by the existence of d holes at Ni sites. Also, d holes should exist at the sites of Cu atoms in alloys containing less than ~55 % Cu. As a result, APS peaks of Cu  $L_{2,3}$  levels were expected in alloys with < 55 % Cu. But Ertl and Wandelt did not observe any peak in the Cu  $L_{2,3}$  region in the alloys. These results led them to conclude that the rigid band model is not valid for this alloy system.

On the basis of one electron model the relative intensities of  $L_3$  and  $L_2$  spectra are expected to be given by the statistical weighting  $2j + 1$ . This predicts an  $L_3/L_2$  intensity ratio of 2. Park and Houston [76] have systematically studied the variation of  $L_3/L_2$  intensity ratio across the first transition series and observed a distinct minimum at Cr. Deviation of the results from the statistical weighting of 2 implies either an anomaly in the excitation probability or j dependent selection rules for the radiative decay of 2p holes. They have excluded the first probability in the case of Cr by observing this ratio from the AEAPS to be exactly 2 [47]. Another effect, known as "resonance", needs to be considered while discussing this ratio for Cr. If the photocathode used to detect the radiative yield contains the same elements as the anode being studied, the intensity ratios of closely spaced levels are expected to be altered. Park and Houston cleaned their samples by sputtering and heating at high temperatures in situ. Cr has the highest vapor pressure among the 3d metals. Therefore, in their experiment, the photocathode

was very likely to be Cr. However, in the absence of experimental work which deals with such a resonance effect, it is safe to conclude that the AEAPS more accurately reflects the relative excitation probabilities of 2p levels since the radiative transition probabilities for these levels are extremely small. The experimental results are, therefore, consistent with the predictions of one electron theory that the excitation probabilities of  $2p_{3/2}$  and  $2p_{1/2}$  levels go as  $2j + 1$ . In the case of rare earths the ratio of the change in the total

overall trend is consistent with the j-j coupling transition rates in rare earths.

Assuming constant transition matrix elements and sharp core hole states, SXAPS gives, within a one-electron approximation, an autoconvoluted picture of the conduction band density of states. The desired density of the unoccupied states is related to the resulting line shape of the SXAPS spectrum in a nonlinear fashion. Dose et al. [20,21,26] have developed a successful inversion procedure for the integral

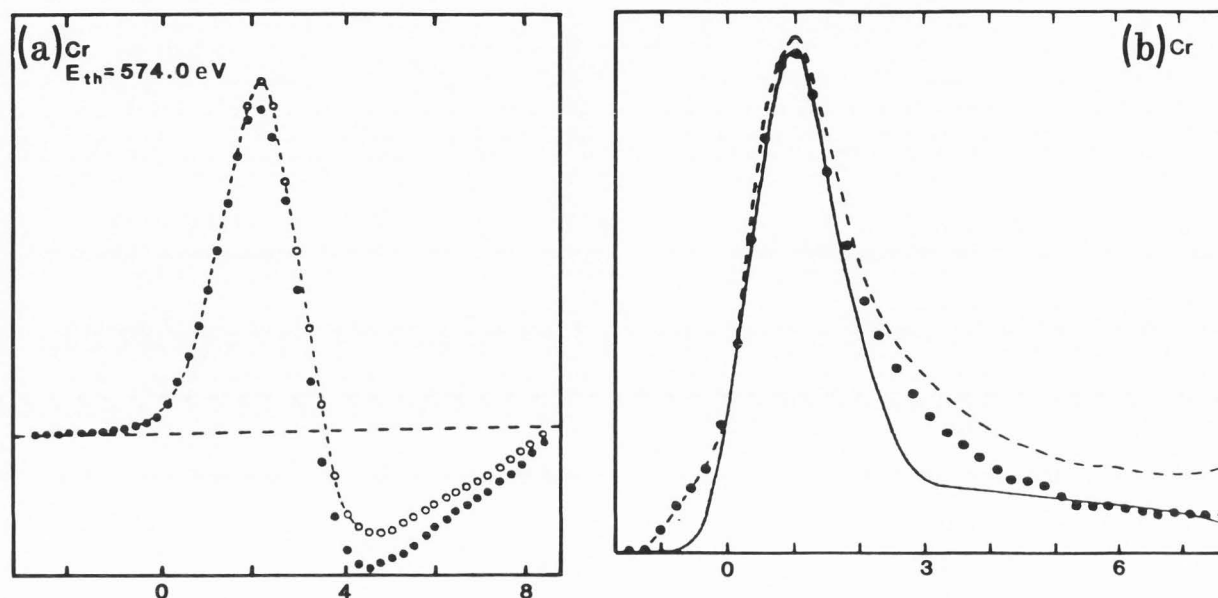


FIGURE 7:  $L_3$ -level APS spectrum of Cr. (a) Open circles indicate measured spectrum. Full circles represent the same spectrum after correction for energy losses. (b) Broken curve represents the density of empty electronic states in Cr. Full circles are the deconvolution of the data (full circles) in fig. (a). The full curve is derived from theoretical calculations. The figures are reproduced by permission from ref. [22].

fluorescence yield of  $M_5$  to the same change of  $M_4$  should be  $3/2$  on the basis of this theory. This is different from the  $L_3/L_2$  ratio obtained for the transition metals. Hua et al. [48] have measured the  $M_5/M_4$  ratio for the rare earth series from SXAPS. They classified this ratio into three groups equal to  $3/2$ ,  $4/2$ , and  $5/2$  across the series. Chopra et al. [15] have, however, found a gradual increase in this ratio with  $Z$ . It seems that for heavier rare earths  $3d_{3/2}$  holes decay via radiative transitions with a smaller probability than  $3d_{5/2}$  holes. Towards the end of the rare earth series this ratio reaches a maximum with Tm and then tends to decrease. The

equation [ equation 8] and derived the density of states for Cr, Fe and Ni from their experimental SXAPS data [22]. Figure 7 shows the density of empty electronic states in Cr obtained by deconvolution of the experimental data. The data have been compared with the DOS derived from the theoretical calculations. Considering the broadening resulting from the energy losses in the sample prior to core hole excitation the overall agreement in the case of 3d transition metals between theory and experiment is very good. The deviations in the region beyond the d band maximum seem to indicate the limits of validity of the correction procedure. They have

## Appearance Potential Spectroscopy

also found [27] good agreement between the theoretical calculations and the experimentally obtained and deconvoluted SXAPS spectra of Hf, Ta and W. Schulz et al. [84] have carried out a highly resolved appearance potential study of polycrystalline ferromagnetic Fe, Co, and Ni. By means of a deconvolution technique developed by them, they found good agreement between the derived DOS from APS spectra of these elements and the single-particle band structure calculations. Dose and Reusing [24] have shown that the structural features in the SXAPS spectra of elemental Co, Ni, and Cu correspond to the structure in the s-p like density of states of these metals. The results, therefore, convincingly demonstrate the potential of SXAPS in combination with the autoconvolution procedure to derive the density of states from the SXAPS line shape.

### Rare Earths

The theory that relates the SXAPS line shapes to the self-convolution of one-electron density of states above  $E_F$  has worked well for the 3d transition metals and some of the simple metals [66,67,76]. The basic assumption of the theory is that both the excited core electron and the scattered projectile electron are implanted in the spatially extended states in the conduction band. However, for rare earths the self-convolution model fails. Considerable discrepancies between theory and experiment have appeared. The breakdown of the one-electron model occurs because the excited core electron may occupy 4f orbital which is quite localized about the excited ion. An interpretation of the SXAPS line shapes in terms of the atomic like transitions, including exchange interaction, rather than in terms of continuous interband transitions, violates the fundamental assumption on which the one electron model is based. To explain the SXAPS of rare earths, Wendin [100] has proposed a two densities of states model: one for the scattered projectile electron and the other for the excited ion with an electron-hole pair. The two densities of states may be interacting or non-interacting with each other. For the projectile electron the DOS is proportional to conduction band states generally represented by the bremsstrahlung isochromat data. The DOS for the core electron is localized and approximated with the soft x-ray absorption measurements. One or both of these may contain highly localized states. This model is no longer appropriate when both the projectile electron and excited core electron occupy 4f orbitals on the same excited ion of  $4d^9 4f^{N+2}$  configuration.

Smith et al. [87] have found an apparent relationship between the portions of SXAPS spectra and the soft x-ray absorption data for rare earths.

We have made a comparative study [14] of  $M_{4,5}$ -levels SXAPS of rare earth metals (fig.8) to understand the trends

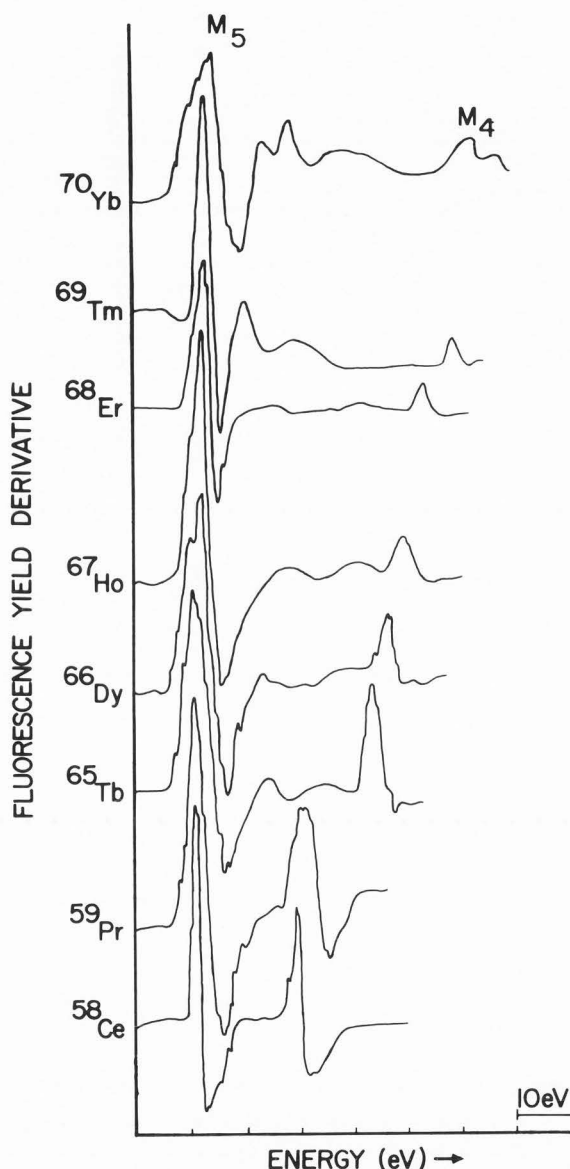


FIGURE 8:  $M_{4,5}$ -levels SXAPS spectra of rare earths. The spectra are aligned for purposes of making comparison. The complexity of the secondary structure is seen to be rich for medium rare earths and decreases for light and heavy rare earths. The figure is reproduced by permission from ref. [14].

across the series. The spectra have been aligned for purposes of making comparison. The peak intensities are not normalized. The  $M_4$  and  $M_5$  spectral region consists of two main peaks superimposed with secondary structure. The complexity of this structure is rich for medium rare earths and decreases for light and heavy rare earths. The intensity of the  $M_4$  peak decreases with  $Z$ . According to one-electron theory the intensity ratio of  $M_5$  to  $M_4$  peaks is computed by the statistical weighting of  $2j + 1$ . For rare earths this ratio is predicted to be 1.5. The systematic study of the SXAPS of rare earths indicates a significant increase of  $M_5/M_4$  intensity ratio towards the end of the series, reaching a maximum with Tm and then tending to decrease. The trend is consistent with the  $j$ - $j$  coupling transition rates in rare earths. As the  $4f$  levels are progressively filled, the radiative probability of  $3d_{3/2} \rightarrow 4f_{7/2}$  transition decreases without affecting the  $3d_{5/2} \rightarrow 4f_{7/2}$  transition probability significantly. The intensity ratio of  $M_5$  to  $M_4$  peaks is predicted to be 1.5 as stated earlier. The deviation of this ratio in the case of rare earth series from the statistically weighting of 1.5 implies an anomaly in the excitation probability. We have also recorded the  $M_2$  and  $M_3$ -level SXAPS of the same elements and found these to be more than an order of magnitude weaker relative to  $M_4$  and  $M_5$  peaks. This indicates that rare earths exhibit intense SXAPS structures for those core levels which have proper symmetry to satisfy dipole selection rules for transitions to the final states.

Any explanation of the SXAPS of rare earths must take into account the local character of the atoms. Some authors [41,87] have proposed the resonant scattering interaction in which both the incident and  $3d$  core electrons occupy the atomic  $4f$  orbitals according to  $3d^{10}4f^N + e \rightarrow 3d^9 4f^{N+2}$  transition where  $N$  varies from 0 for La to 14 for Yb. This implies that SXAPS are not predicted for rare earths with less than two  $4f$  vacancies. However, SXAPS spectra of rare earths with less than two  $4f$  vacancies have been observed by Chopra and Martin [14]. The systematic investigations of the rare earths [14,41] also reveal some clues regarding the excitation probabilities of various transition channels.  $Tm^{69}$  (ground state  $3d^{10}4f^{12}$ ) may assume either of the final state configurations:  $3d^9 4f^{14}$  or  $3d^9 4f^{13} \epsilon f$  (where  $\epsilon f$  is the continuum state) depending on the scattering modes of the incident and excited core electrons. Tm SXAPS yields a strong  $M_5$  peak which is not rich in complex line structure. The next element  $Yb^{70}$  is divalent and has no  $4f$  vacancy. However,

$Yb_2O_3$  has been reported to be trivalent with  $4f^{13}$  configuration. The measured  $M_5$ -level SXAPS from oxidized Yb surface is quite broad and complex, and is approximately 15 to 20 percent in intensity relative to the Tm peak. It is obvious that resonant process which scatters both electrons into the  $4f$  state is not valid in  $Yb_2O_3$  which has only a single  $4f$  vacancy. The SXAPS spectrum of  $Yb_2O_3$ , therefore, results from the second resonant process of the scattering of two electrons to the final state configuration  $4f^{14} \epsilon f$ . From the comparison of  $M_5$ -level SXAPS of  $Yb_2O_3$  with that of Tm, it is estimated that the oscillator strengths of the  $M_5$ - or  $M_4$ -level SXAPS peaks is divided between the  $3d^9 4f^{N+2}$  and  $3d^9 4f^{N+1} \epsilon f$  configuration states in the ratio of 5 : 1, based on the peak intensities.

The exchange interaction between the  $4f$  electrons and  $3d$  hole splits the final state configuration into a multiplet. The multiplicity of these levels, however, depends entirely on the number of  $4f$  electrons and is maximum when the  $4f$  levels are half full. The exchange interaction in the case of the  $3d$  levels of rare earths is weaker than the spin-orbit interaction. The observed line structure is, therefore, grouped around the spin-orbit components and constitutes a small fraction of total oscillator strength of the  $3d$  excitation. The line structure is then expected to get quite complex for medium rare earths and then to tend to decrease towards the extreme ends of the series. This is, indeed, demonstrated by the data of the present investigation.

The exchange interaction plays a more dominant role in the  $4d$ - $4f$  transitions for the rare earths. The spin-orbit splitting is rather weak. The multiplet splitting is expected to be more pronounced when the  $4d$  level is excited. As a result of the strong exchange interaction between the  $4d$  vacancy and  $4f$  electrons, the final state splits into a multiplet spread over 20 eV. Each of the final state configurations consists of a large number of terms, and the number of possible transitions to these terms is large. The observed SXAPS spectra for  $N_{4,5}$  levels of rare earths are, therefore, quite complex [10]. The detailed theoretical calculations of the convoluted bands with the multiple splitting due to exchange interaction in the presence of an extra electron are needed for more plausible interpretation of these spectra.

Shulakov et al. [86] have studied in the La  $N_{4,5}$ -region the ultrasoft x-ray emission spectra of lanthanum oxidized in vacuum. The spectra were

## Appearance Potential Spectroscopy

taken at various incident electron energies. New structural features appeared in the spectrum with increasing electron energy. Based on dipole selection rules, the various peaks in the radiation spectrum have been attributed to the radiative decay via the new states formed for x-ray emission. They have compared these features with those in the isochromat spectra of  $\text{La}_2\text{O}_3$ . The integrated bremsstrahlung intensity was found to increase monotonically with the electron energy. This variation in the intensity is responsible for the structure of the APS spectrum and may arise near the thresholds because of anomalies in the cross section for the inelastic scattering of electrons into free electron states of the target. They conclude that the main contribution to the fine structure of the La  $N_{4,5}$  APS spectrum comes from the characteristic 5d-5p and bremsstrahlung channels. The resonance lines in the 4d emission spectrum of La are usually associated with transitions to the ground state from highly localized excited states below the threshold. The features observed in the  $N_{4,5}$  APS spectrum have been very well accounted for by the principal channels of radiative decay of a 4d vacancy in the x-ray emission spectrum. This study demonstrates that the x-ray emission spectrum of La can very well be used to explain the structures associated with its APS spectrum.

### Intermetallics

Valence band spectroscopies (AES and XPS) are practically limited to binary alloys because of the complications encountered with the increase in the number of alloy constituents. In contrast to AES and XPS which probe the occupied DOS of the sample, SXAPS measures the unoccupied conduction band DOS. An important aspect of SXAPS should be pointed out in the present context. Since the matrix element governing the core hole creation involves very short range wave function of initial core electron state, the technique is expected to reveal a localized DOS. Since the spectra of different constituents is well separated in energy, the application of SXAPS is by no means limited to binary alloys. The changes in SXAPS spectral features and shifts in BE which accompany alloy formation will better characterize the alloys.

Metallic glasses are believed to be normally void of crystal periodicity and exhibit band structure changes on crystallization [23]. Dose and Haertl report the SXAPS measurements on metallic glass  $\text{Co}_{58}\text{Ni}_{10}\text{Fe}_5\text{B}_{16}\text{Si}_{11}$  (Vitrovac 6010) [23]. They observed satellites in the

elemental  $L_3$  SXAPS of Ni, Co, and Fe and interpret them as being characteristic of long range order since they do not show in either amorphous or crystalline states of the alloy. These spectra obtained in the amorphous state of the alloy exhibit certain changes. Nickel spectrum shows considerable broadening of the d band peak, whereas Co and Fe spectra remain practically unchanged in this part of the spectra. All three spectra differ in the region of the signal dominated by s partial density of states. The ratio of s to d partial DOS is in all three cases considerably higher in the alloy than in the pure samples. On crystallization, of the alloy in situ, the boron spectrum shows dramatic changes including a large core-level shift. The spectra of amorphous states is characteristic of a pure s band. On crystallization it contributes significantly to the local s partial DOS at the Co and Fe atom sites. The observed spectra of Co and Fe indeed exhibit small but distinct changes indicating an increase in the s partial DOS at the respective atom sites. The spectra of Ni and Si, however, do not change on crystallization. Overall the application of SXAPS to metallic glass reveals a lot of information regarding the electronic structure which is not accessible by other spectroscopic techniques. Moreover, this application shows that SXAPS, not limited to binary alloys, is particularly suitable for the study of multicomponent systems.

We have utilized the SXAPS technique to study the rare earth-transition metal intermetallics [12,13,43,44]. Most of La-Ni intermetallics are found to be paramagnetic. The paramagnetic susceptibility can be accounted for solely in terms of the La component, while Ni is assumed to be non-magnetic. Alloying Ni with electron-rich La diminishes the Ni magnetic moment progressively as the La content increases. Traditionally this has been ascribed to the filling of the Ni d-band by extra electrons supplied by La. XPS studies, however, indicate that despite band filling, there is no evidence of large charge transfer [45]. Ni has only 0.6 d vacancies, and Ni spectra should reflect complete filling of 3d band at high La concentration as a result of charge transfer. Hatwar and Chopra [43] have investigated the SXAPS of La-Ni intermetallics. Since SXAPS probes the local density of unfilled states, any vacant d-states in Ni band of the intermetallics will be reflected in the Ni SXAPS spectra. The changes in spectral features of SXAPS will give information about the charge transfer and hybridization of the valence bands of the constituents. Since La  $3d_{3/2}$  and

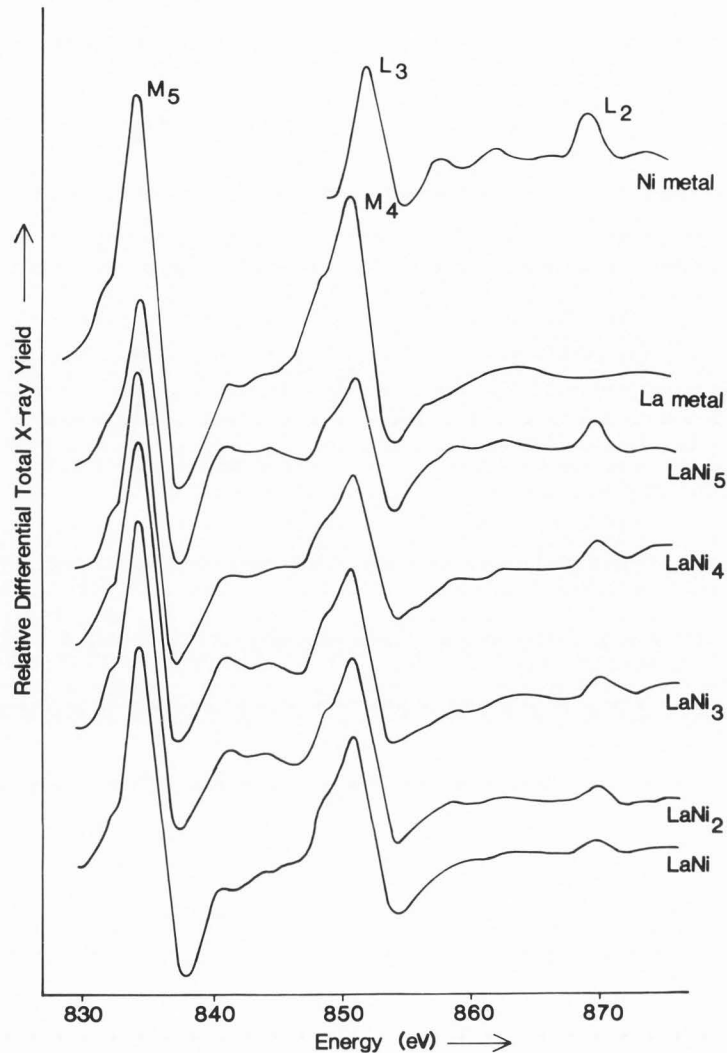


FIGURE 9:  $M_{4,5}$ -levels of La and  $L_{2,3}$ -levels of Ni SXAPS spectra in pure metals and their intermetallics. The figure is reproduced by permission from ref. [43].

Ni  $2p_{3/2}$  have nearly the same energy and their SXAPS peaks overlap, Ni  $L_2$  peak was used to gain information regarding the electronic structure of these intermetallics. The spectra of  $\text{LaNi}_x$  ( $x = 1$  to  $5$ ) were investigated and are shown in fig.9. The intensity of Ni  $L_2$  peak decreases as the concentration of La increases (i.e., going from  $\text{LaNi}_5$  to  $\text{LaNi}$ ). The band structure calculations of  $\text{LaNi}_5$  indicate the transfer of 1.5 electrons per La atom to Ni [62]. The 1.5 electrons will be sufficient to fill the 0.6 d hole of Ni in  $\text{LaNi}$  and 1.2 d holes of Ni in  $\text{LaNi}_2$ . As a result we should not expect Ni  $L_2$

SXAPS in these intermetallics. However, in no case a complete disappearance of Ni  $L_2$  peak was observed. The appearance of Ni  $L_2$  peak consistently in all the La-Ni intermetallics indicates the presence of the 3d unoccupied states in the conduction band of Ni. The mere charge transfer is, therefore, not considered adequate to explain the present SXAPS results. BIS of pure La shows a peak at  $\sim 5$  eV above  $E_F$  corresponding to 4f states [55]. At this energy the variation in DOS of Ni are minimal [89]. According to the joint density of states model the APS spectra

## Appearance Potential Spectroscopy

of Ni (as well as of La) should show, apart from the threshold peak, a structure for the peak in DOS at  $\sim 5$  eV above  $E_F$ . Since no such structure has been observed in SXAPS spectra of La and Ni in La-Ni system, it is logical to conclude that the joint density of states model fails to account for the bonding in these intermetallics. As an alternative explanation, the effect of hybridization of La and Ni wave functions needs to be considered for the partial filling of 3d band. The hybridization of La and Ni bands results in a consequent filling of the band without appreciably changing the d count of Ni. In conclusion, the observation of Ni  $L_2$  peak in all La-Ni intermetallics indicates that the hybridization of La and Ni bands is more important for filling the 3d band of Ni than charge transfer. Dose et al. [25] have considered the effect of hybridization in glassy  $Cu_{60}Zr_{40}$  sample studied by SXAPS. Pure Cu spectra shows a nearly step-like behavior superimposed with some oscillatory structure. The Cu spectrum in the glass resembles that of partially filled d-shell transition metals. They interpreted this SXAPS spectra of Cu as a result of hybridization of Cu d-states with the p-states of Zr.

### Adsorption

The surface electron spectroscopies are powerful experimental methods for investigating the sorption process. In DAPS, electrons which are backscattered quasi-elastically are measured. On the other hand, AEAPS detects the yield of secondary electrons produced by primary electrons. In general, the sensitivity of the DAPS differs from that of AEAPS, and DAPS has higher sensitivity in the neighborhood of the surface. Since the back-scattered electrons in DAPS travel at least twice the path corresponding to the penetration depth, the probing depth in DAPS spectra is estimated to be about half of that in the AEAPS spectra [71]. The differences in the DAPS and AEAPS spectral measurements on the same solid specimen should therefore give information about the depth distribution of the diffused gas atoms into the surface. Konishi et al. [52] have utilized this technique to determine the penetration of oxygen and nitrogen atoms into Ti surface as a function of exposure to the gases. Their measurements show that the DAPS  $L_3$  negative peak heights saturate at an oxygen exposure of 80 L, while the AEAPS peak heights continue to increase up to an exposure of 100 L. The Ti  $L_3$  peak heights of both DAPS and AEAPS spectra saturate at a nitrogen exposure of about 10 L. Since Ti  $L_3$  negative peak height is a measure of degree of overlap of Ti 3d

and gas ( $O_2$  and  $N_2$ ) 2p wave functions, the study concluded that the saturation values of the diffusion depths of nitrogen atoms in Ti thin films are much smaller than those of oxygen atoms.

SXAPS has also been utilized to study the adsorption phenomena. The SXAPS spectra of 3d metals when exposed to oxygen showed [3] different oxygen 1s spectra for chemisorbed oxygen and for oxygen in the oxide. Chemisorption is characterized by one single peak in the oxygen 1s spectra and no change in the metal 2p spectra. Thus chemisorption and oxidation phases can be distinguished with the help of SXAPS.

The SXAPS spectra as obtained by Nyberg [68] in the case of Ti exposed to oxygen is shown in fig.10. The signal strength in the oxygen 1s spectra continues to increase upon exposure. Around 10 L of exposure some changes start to occur in the spectra. These mark the start of the formation of the oxide because the electronic structure changes when an oxide starts to grow on the surface. During the chemisorption stage the metal 2p spectra remain unchanged while appreciable changes occur during oxide formation [2,34]. It should be noted that the density of states effect is suppressed in AES by using large modulation voltages when taking the derivative. This AES detection scheme also makes it difficult to distinguish clearly between the chemisorption stage and the oxide formation stage by simply looking at the shape of the spectra. The SXAPS study of oxygen adsorption has been also extended to Cr, Fe and Ni [68]. Andersson and Nyberg [4] have also studied the chemisorption of C, N and S on these transition metals. They have interpreted the peak in the spectra in terms of unoccupied valence states of the substrate-adsorbate complex. Also, the full width at half maximum (FWHM) of the peaks has been found to correlate with the variation in the width of the unfilled portion of the substrate 3d band. APS, thus, provides a simple means for studying the kinetics of the reaction of gases with 3d-transition metals. The most striking advantage of the technique is the possibility of distinguishing clearly between the chemisorption stage and the oxide formation stage -- a feature not directly available by other techniques.

We have also studied the La and  $LaH_3$  by AEAPS [in press] with the view that this type of study would be helpful in understanding the hydrogen absorption process in La and also in  $LaNi_5$ . The  $M_{4,5}$ -levels spectra are shown in fig.11. The spin-orbit splitting in the case of La is found to be 16.5 eV. In the pure

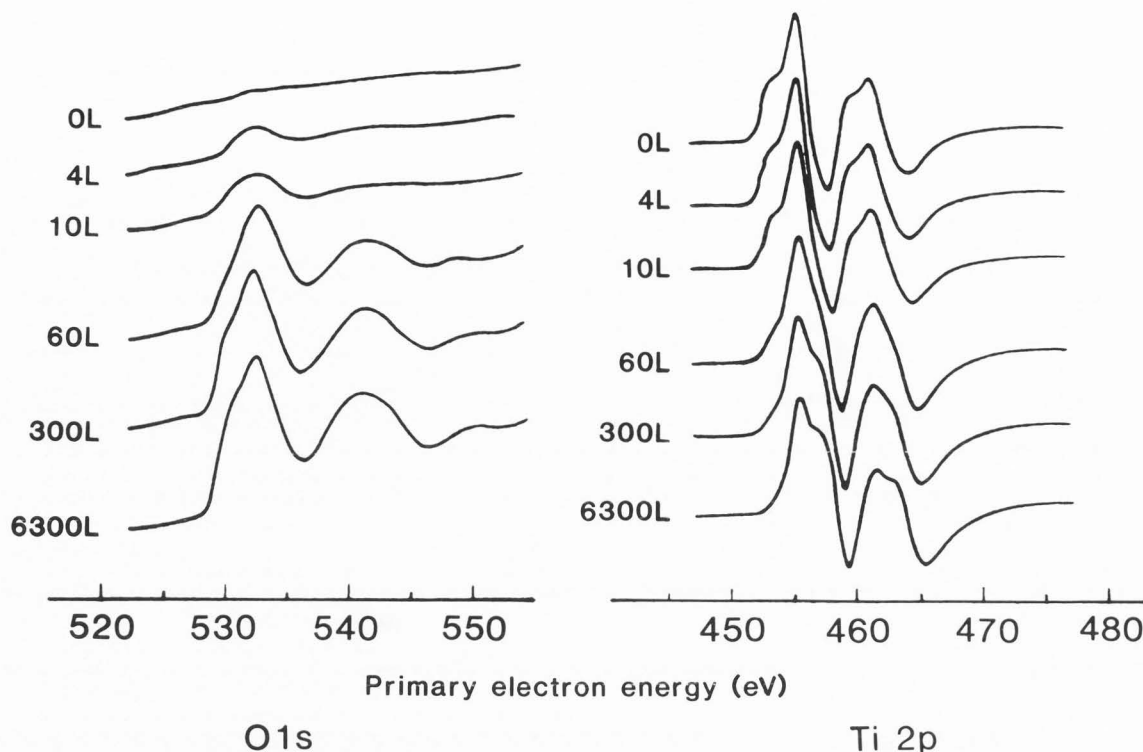


FIGURE 10: Oxygen 1s and titanium 2p spectra for different oxygen exposures. Chemisorption stage is characterized by one single peak in the oxygen spectra and no change in the metal spectra. Upon oxidation the spectra change. The figure is reproduced by permission from ref. [68].

metal each spin-orbit level is seen to give rise to two structures : a shoulder-like peak (A) followed by a more intense peak (B) which is accompanied by an undershoot. The peak A reflects the excitation  $3d^{10} \rightarrow 3d^9 4f^1$  while the peak B the excitation  $3d^{10} + e \rightarrow 3d^9 4f^2$  [101]. In the XPS 3d-level spectra of La a similar structure on the low energy side of the main peak is observed [70,83]. This has been interpreted as due to the lowering of the 4f level in the presence of a 3d hole. Based on the screening mechanism, the low energy structure is shown to correspond to the well screened ( $3d^9 4f^1$ ) hole whereas the main peak is due to the poorly screened ( $3d^9 4f^0$ ) final states [36]. As a result, we have drawn a qualitative picture based on the one-electron process, as shown in fig.12. As the energy of the incident electron is increased, excitation of a 3d electron becomes possible. Since the 4f-levels are localized in the core region, they are sensitive to their mutual repulsion and to the attractive Coulomb potential

of the 3d hole. As a result, the 3d hole pulls the empty 4f level down 1.2 eV below  $E_F$ . The 3d-excitation then becomes possible, as shown in fig.12a. This gives rise to peak A in fig.11. Increasing the incident electron energy further, both the incident and the core electrons may go into the strongly localized 4f levels which, due to the 4f-4f repulsion are raised above  $E_F$ . This situation is shown in fig.12b and corresponds to peak B in fig.11. From the measurements, we estimate the position of the 4f level in this excited configuration of pure La as 1.5 eV above  $E_F$ .

In the AEAPS spectra of La in  $LaH_3$ , shown in fig.11, three peaks C, D and B' are observed in the  $M_5$  region. Comparison of this with the metallic spectrum shows the absence of the peak A and the existence of two additional peaks C and D on the low energy side of the main peak B'. One of these additional peaks is due to the pulling down of the 4f level in the presence of a 3d

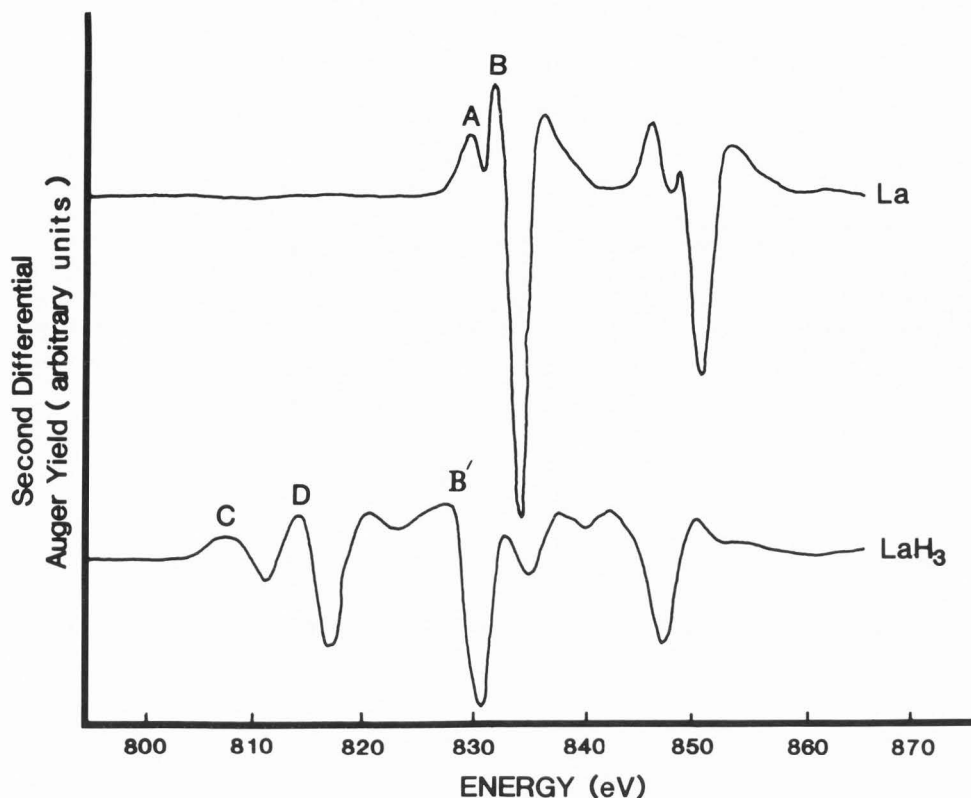


FIGURE 11:  $M_{4,5}$ -levels AEAPS spectra of La in pure metal and in  $LaH_3$ . Comparison of the two spectra shows the absence of the shoulder A to the main peak and the presence of two additional peaks (C and D) on the lower energy side.

hole, and the other is due to the hydrogen induced band. In the case of insulating La compounds, the XPS spectra exhibit a satellite on the high BE side of the main peak. This has been interpreted [17] as the lowering of the 4f level to a few eV above the ligand derived band. However, no high BE satellite is observed in the AEAPS spectra for  $LaH_3$ . This implies that the model for insulating La compounds is not applicable to  $LaH_3$ . Therefore in the case of  $LaH_3$ , the 4f levels are pulled down below the hydrogen induced band. On the basis of this the peak C is then assigned the transition of the 3d electron to the pulled down 4f level below the hydrogen induced band and the peak D the transition to the hydrogen induced band. A tentative energy level diagram drawn for these possible transitions is shown in fig.13. In fig.13a is shown the presence of a 3d hole and the consequent pulling down of the 4f level

below the hydrogen induced band. In fig.13b is depicted the transition giving rise to peak C in fig.11. The transition corresponding to peak D in fig.11 is shown in fig.13c and reflects the excitation of the 3d electron to the hydrogen induced band. The main peak B' occurs when both the incident and the core electrons undergo resonant transition to the strongly localized 4f levels above  $E_F$  and is shown in fig.13d. From the measurements, we estimate the position of 4f level in the present excited configuration of La in  $LaH_3$  to be 4.1 eV above  $E_F$ . Thus, AEAPS spectra are useful in determining the position of the 4f levels relative to  $E_F$  in rare earths and their hydrides. Such a determination of the position of 4f levels is extremely important in understanding the applications, such as superconductivity and permanent magnetism, of rare earths in modern technology.

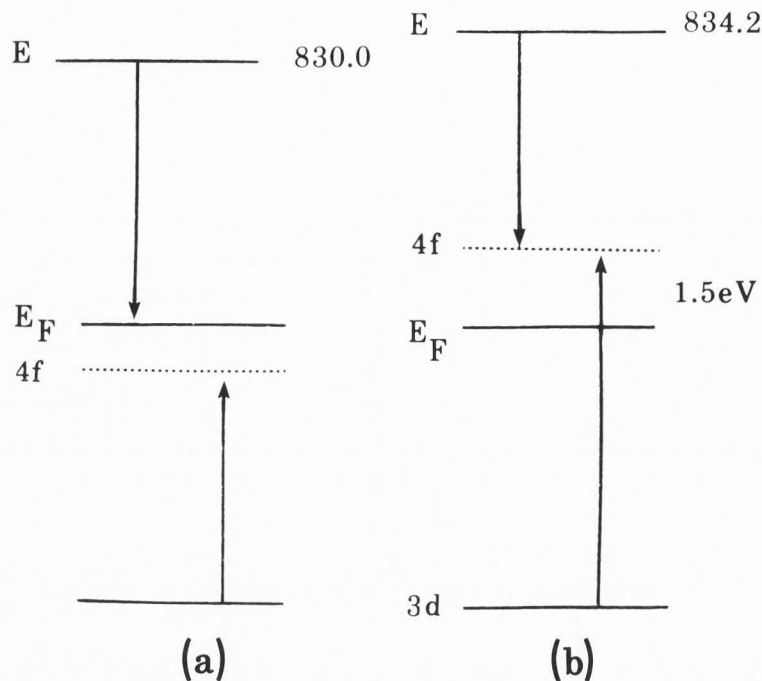


FIGURE 12: One electron band picture with different 4f levels for 3d excitation in metallic lanthanum. (a) 4f level pulled down below E<sub>F</sub> in the presence of a 3d hole. (b) Both incident and core electrons go into the strongly localized 4f level above E<sub>F</sub>.

### Fine Structure

The extended x-ray absorption fine structure (EXAFS) associated with an x-ray absorption discontinuity has proved in recent years [16,59,91] a reliable technique for obtaining structural information in a system. The information obtained includes the interatomic distance, coordination number, and degree of disorder. In contrast to the bulk information available from the EXAFS data, extended appearance potential fine structure (EAPFS) gives information about the surface structure since it utilizes low energy electron beam for excitation. The fine structure is obtained by recording the APS spectra as a function of primary electron energy [73]. The structure occurs on the high energy side of a particular core level appearance potential edge and extends over several hundred eV. This structure appears as a result of a spherical wave emanating from the central atom, modified by weak backscattering from nearby atoms. Recent work has shown EAPFS to be analogous to EXAFS [7,57,58]. Therefore, the analysis

of EAPFS is carried out in much the same way as for EXAFS. After the background subtraction, the fine structure  $\chi(k)$  is plotted as a function of free momentum of the excited core electrons via the equation:

$$\hbar k = [2m(E - E_0)]^{1/2}. \quad (13)$$

Here E corresponds to the energy of primary electron, and E<sub>0</sub> is the BE of the core level involved. The Fourier transform of  $\chi(k)$  yields a radial structure function:

$$F(r) = \int_{k_{min}}^{k_{max}} k^3 \chi(k) \exp(-2ikr) dr. \quad (14)$$

The nearest neighbor distance of the surface constituents is easily obtained from the prominent peak position after appropriate corrections for phase shift and multiple scattering as in EXAFS [90]. These phase shifts are due to both the central atom and the surrounding backscattering atoms. These depend on the angular momentum of the outgoing electron wave function. In EXAFS, photon excitation implies a dipole selection rule, greatly simplifying the determina-

Appearance Potential Spectroscopy

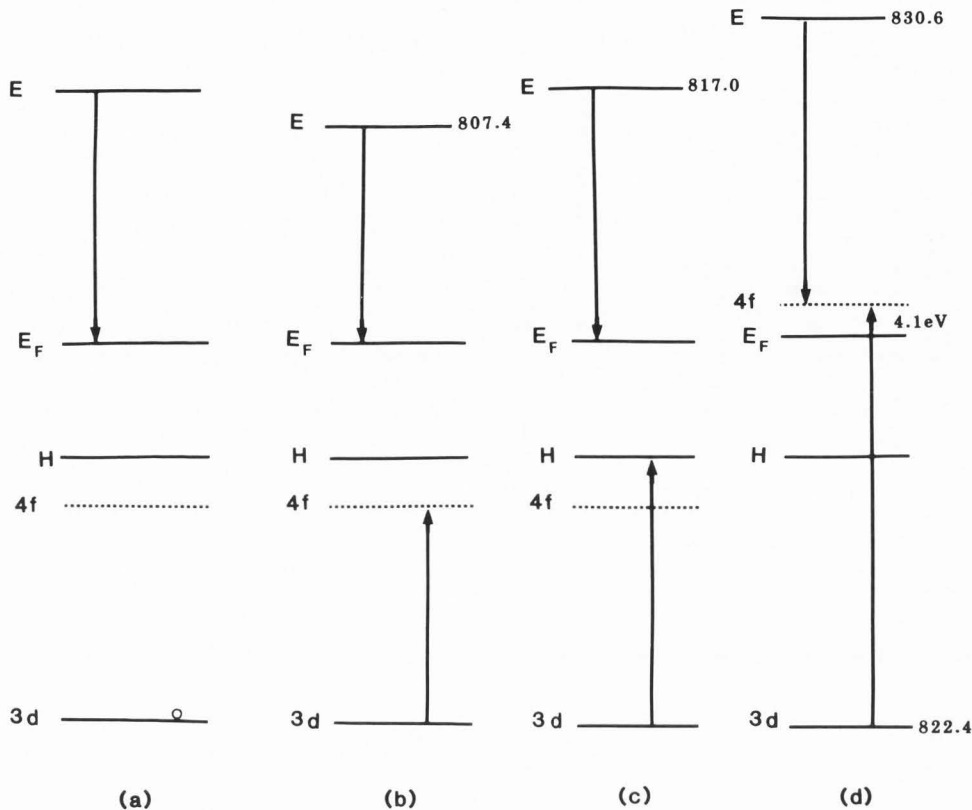


FIGURE 13: One electron band picture for 3d excitation in  $\text{LaH}_3$ . The 4f level in different situations is shown. (a) The 4f level is pulled down below the hydrogen induced band. (b) The 3d excitation into the 4f level giving rise to peak C in fig. 11. (c) The 3d excitation into the hydrogen induced band giving rise to peak D in fig. 11. (d) The incident and 3d electrons going into the 4f level above  $E_F$ , corresponding to peak B' in fig. 11.

tion of this angular momentum and hence of the appropriate phase shifts. In EAPFS, however, the major question in the analysis is the angular momentum of the two final state electrons [31]. The knowledge of the phase shifts which is a function of the angular momentum of the electrons determines the precision to which the nearest neighbor distances can be resolved. In their model calculations Mehl et al. [63] have suggested a pseudodipole excitation rule for EAPFS, i.e., the data can be analyzed with the same phase shifts as would be used for EXAFS. Using this proposed model for the K edge of Al and  $L_3$  edge of Ti, they have determined the distance of the first shell from the origin within  $\pm 0.004$  nm for Ti and  $\pm 0.001$  nm for Al. This

success encourages EAPFS to be used as a valid tool in surface measurements since theoretical phase shifts for all the elements have been calculated [94] and successfully employed in EXAFS analysis.

Konishi et al. [53] have measured the EAPFS spectra for polycrystalline Cr using the AEAPS spectra. The fine structure was recorded in the second derivative mode. In fig.14 is shown the magnitude of the Fourier transform of the fine structure obtained by them above the  $L_1$  appearance potential edge of polycrystalline Cr. Using the phase shifts calculated by Teo and Lee [94], they determined, in the case of Cr, the nearest neighbor atomic spacing as 0.253 nm ( $l = 0$ ), 0.254 nm ( $l = 1$ ) and 0.254 nm ( $l = 2$ ) in good agreement with bulk

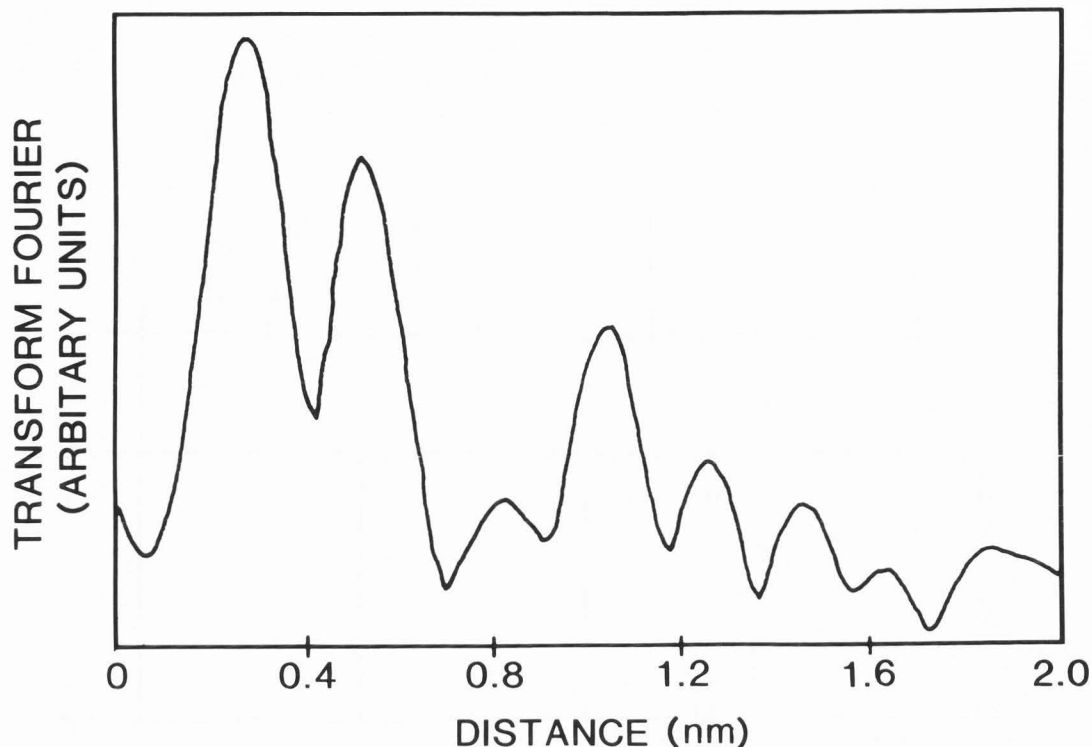


FIGURE 14: The magnitude of the optical Fourier transform of the extended fine structure above the  $L_1$  appearance potential edge of polycrystalline Cr for  $l=0$ . The prominent peak is at  $0.233 \pm 0.01$  nm. The nearest neighbor atomic spacing  $0.253 \pm 0.01$  nm is in good agreement with that for bulk values. The figure is reproduced by permission from ref. [53].

value (0.250 nm).

Boer et al. [7] have studied the adsorption of oxygen on Al(100) using DAPS. The (100) face of Al was exposed to 120 L of oxygen. They concluded from the fine structure associated with the O K-edge that oxygen in the system is not above the surface but rather between the first (top) and second layers. The oxygen-aluminum distance is determined [30] to be  $0.198 \pm 0.05$  nm. In bulk  $Al_2O_3$ , there are two O-Al separations, 0.186 nm and 0.197 nm. The larger one is because of the oxygen lying between two Al atoms while the small one is because of the oxygen between an Al and a vacancy in the chain. Stohr et al. [92] studied the 3 nm thick film of oxide on Al foil by surface EXAFS (SEXAFS) and found a spacing of 0.191 nm, the average of the two bulk values. This clearly demonstrates the surface sensitivity of EAPFS. Boer et al. [8] studied the oxygen-nickel system. The (100) face of Ni was exposed to oxygen, and DAPS spectra were

observed. They observed a peak in the Fourier transform at 0.204 nm using  $l = 2$  phase shifts. This peak lies respectively at 0.227 or 0.221 nm when  $l = 0$  or  $l = 1$  phase shifts are used. The bulk Ni-O separation is 0.209 nm. They conclude that two or three final state partial waves contribute to the fine structure.

The major complication in EAPFS is diffraction oscillations due to elastically scattered electrons from ordered regions of the sample. This can be overcome by monitoring soft x-ray emission during the core de-excitation. However, for the soft x-ray levels, the probability for this SXAPS process is less than one percent. It is, therefore, important to detect the x-rays with high quantum efficiency to minimize the effects produced due to the incident electron current. High quantum efficiency has been achieved with a nude solid state surface barrier detector consisting of a  $\langle 111 \rangle$  oriented Si crystal coated with a thin Al layer and cooled

by liquid nitrogen [2]. Such a detector has been utilized by Einstein et al. [30] in their study.

EAPFS has been found to achieve good signal-to-noise ratio up to at least  $110 \text{ nm}^{-1}$ , i.e., approximately 500 eV above the threshold, the upper limit of typical EAPFS measurements [64]. On the other hand, SEXAFS signals are difficult to resolve above about  $80 \text{ nm}^{-1}$  [93]. EAPFS has also been successful in providing structural information on the oxidation of Al [7] and Ni [8] where the LEED patterns were found to be extinguished upon exposure of metal surfaces to oxygen. While the K edge spectra have been fairly informative, more theoretical data seem to be necessary for the analysis of the L edge spectra [8].

EAPFS is produced by backscattering from close neighbors of the excited atom and thus probes only very short-range order. It is, therefore, ideally suitable for systems lacking long-range order. EAPFS experiments do not have stringent requirements of sample regularity and purity. In contrast to EXAFS, EAPFS can obtain fully adequate signal strength from a relatively thin adsorbate layer. Thus, it probes features distinctly characteristic of the surface region. EXAFS experiments require high intensity x-ray sources such as those available from synchrotron or rotating anode tubes. These are not commonly available in laboratories. EAPFS experiments use equipment which is commonly accessible in most surface science laboratories thus making it a widely available option for fine structure measurements.

### Summary

In this review paper we have discussed the interesting applications of APS to modern science and technology and highlighted its importance relative to other techniques available. In this section, we discuss the relative strengths and limitations of APS.

The intensity of a signal in an APS spectrum is determined by the transition of a core electron to the unoccupied states above the Fermi level. The strength of the signal, therefore, depends upon the density of these unoccupied states. For simple metals, the 3d transition metals, the rare earths, etc., having high density of unoccupied states at the Fermi level, this technique is particularly suitable for their study. Noble metals, such as Au, having very low DOS, give a very weak signal in the spectrum. This is the reason why APS cannot be used as a common analytical tool. For the elements to which it is sensitive the spectra are much simpler and easier to interpret. Moreover, APS is

a non-dispersive technique and requires only relatively simple and inexpensive apparatus. These are the special advantages of APS over other techniques.

The one-electron theory discussed previously explains satisfactorily the features observed in the spectra of simple and 3d transition metals. The theory is valid for systems having continuous DOS above  $E_F$ . Discrepancies between theory and experiment were observed for rare earths, light elements and 4d transition metals. The breakdown of the theory for these materials is due to the assumption that the incident and/or the excited core electrons occupy spatially extended states in the conduction band. Wendin [100] has made an attempt to explain the spectral features on the basis of a model incorporating two densities of states, one for the scattered projectile electron and the other for the excitation with an electron-hole pair. This model is able to explain some of the spectral features. More theoretical work, taking into account the core-level widths, core-hole lifetime broadening, many-body and other effects contributing to the spectrum, is needed to provide a more plausible explanation for the APS spectra.

An interesting application of APS is the derivation of the density of states from the signal shape. Results for 3d and 5d metals have been found in excellent agreement with theoretical calculations. On the other hand, BIS offers the possibility of relating directly the experimentally determined spectral features to the theoretical DOS. APS is found more suitable to the study of intermetallics, especially to multicomponent systems. Another important application of APS is to the study of the adsorption phenomenon. The adsorption of oxygen on certain metal surfaces has shown that there is a change in the oxygen spectra when the oxide formation starts. Thus, it is possible to distinguish the adsorption and oxide formation stages directly from the spectra. In other techniques, e. g., as in AES, such a direct result cannot be obtained by simply looking at the shape of the spectra.

The fine structure (known as extended appearance potential fine structure, EAPFS) occurs on the high energy side of a particular core level appearance potential edge and is analogous to the bulk phenomenon EXAFS in obtaining structural information. The analysis of EAPFS can be done on similar lines as with EXAFS. Unlike EXAFS, which requires high intensity sources such as those from synchrotron or rotating anode tubes, EAPFS makes use of experimental

set-up commonly available in any surface analysis laboratory. Moreover, the structural information obtained from EAPFS is about the surface only. Thus EAPFS is a suitable option for fine structure measurements. The theoretical data available are suitable for the analysis of the K edge spectra of the elements. Additional theoretical data are necessary for the analysis of the L edge spectra. The diffraction oscillations due to elastically scattered electrons from the single crystals pose a complication in EAPFS. This can be overcome by using SXAPS. However, for the detection of x-rays high quantum efficiency detectors must be used.

For surface studies it is necessary to prevent changes of the surface resulting from heating due to primary electrons. This means that low primary currents should be used. SXAPS requires large current and hence can be used in cases where surface changes are not expected to occur due to heating of the sample. AEAPS, on the other hand, uses lower primary currents. Also, the probability of Auger process is approximately two orders of magnitude higher than the probability of x-ray emission in 0-2000 eV energy range of the analysis. Thus AEAPS is more sensitive and is, therefore, commonly used for surface analysis. It must be noted that the structures observed by SXAPS and AEAPS spectra may differ largely because of the core hole decay mechanisms following the excitation of the core electrons in these spectroscopies. In SXAPS the X-ray emission is slow and core hole production and de-excitation are only weakly coupled. On the other hand, in AEAPS the Auger decay is fast and the excitation and decay are strongly coupled. This may lead to some broadening of structure in AEAPS. Dose et al. [19] have observed in solid Ni the smearing of threshold slope and structure in the AEAPS spectrum as compared to the SXAPS spectrum. APS is, however, not limited to solid metals only. With proper experimental arrangement it could be extended to the study of liquid metals, as has been demonstrated by Dose et al. [19].

The major problem in APS is the signal-to-noise ratio. However, better sensitivity could be achieved, in the case of SXAPS, by using energy detectors with high quantum efficiency and by geometric arrangement of the different components of the spectrometer. The disadvantage of signal-to-noise ratio does not limit the use of APS. It has been observed that APS has important advantages unique to this threshold spectroscopy as compared with other surface sensitive techniques, especially with respect to the most widely used AES

[49]. In AES, the backscattering effects describing the intensity enhancement due to energetic scattered or secondary electrons, can introduce serious distortions in quantitative analysis and microanalysis. These distortions do not exist at the excitation threshold and are therefore absent in SXAPS, AEAPS and DAPS, making these spectroscopies more adaptable for the study of surfaces.

The present experience with this technique is quite limited. The experimental work has been narrowed down due to the non-availability of sufficient theoretical data. The main difficulty is the extraction of relevant information from the experimental data in order to correlate with the existing theoretical models. Wide scope exists for the theoretical and experimental work in this field. When the different aspects of APS are fully exploited, this spectroscopy will be accepted as a popular technique for materials characterization of surfaces.

#### Acknowledgments

The authors gratefully acknowledge the financial support from the Robert A. Welch Foundation, the Texas Advanced Technology Research Program, and the American Chemical Society, PRF. The authors wish to thank Dr. Richard Tuerk, Darrell Beauchamp and Mona Towne for their assistance in the final phases of this work. Thanks are also due to the publishers/authors for their permission to use the figures in this paper.

#### References

1. Anderson CR, Lee RN, Morar JF, Park RL. (1982) Comparison of APS and FRESCA core level binding energy measurements, *J. Vac. Sci. Technol.* **20**, 617-621.
2. Andersson S, Hammarqvist H, Nyberg C. (1974) A low noise soft x-ray appearance potential spectrometer and its application to chemisorption of oxygen on nickel, *Rev. Sci. Instrum.* **45**, 877-881.
3. Andersson S, Nyberg C. (1974) Soft x-ray appearance potential spectroscopy of O chemisorbed on Ti, Cr, Fe and Ni, *Solid State Commun.* **15**, 1145-1148.
4. Andersson S, Nyberg C. (1975) Soft X-ray appearance potential spectroscopy of C, N, O, and S chemisorbed on some 3d transition metals, *Surf. Sci.* **52**, 489-504.
5. Bambynek W, Crasemann B, Fink RW, Freund HV, Mark H, Swift CD, Price RE, Rao PV. (1972) X-ray fluorescence yields, Auger and Coster-Kronig transition probabilities, *Rev. Mod. Phys.* **44**, 716-813.
6. Bearden JA, Burr AF. (1967)

## Appearance Potential Spectroscopy

- Reevaluation of X-ray atomic energy levels, *Rev. Mod. Phys.* **39**, 125-142.
7. denBoer ML, Einstein TL, Elam WT, Park RL, Roelofs LD, Laramore GE. (1980) Extended appearance potential fine structure analysis: Oxygen on Al (100), *Phys. Rev. Lett.* **44**, 496-500.
8. denBoer ML, Einstein TL, Elam WT, Park RL, Roelofs LD, Laramore GE. (1980) Extended appearance potential fine structure analysis of oxidized metal surfaces, *J. Vac. Sci. Technol.* **17**, 59-62.
9. Bradshaw AM. (1974) Appearance potential spectroscopy and related techniques, in: *Surface and Defect Properties of Solids*, Chemical Society, London, Vol. 3, 153-183.
10. Chopra D. (1987) Core level spectroscopy of the 4f states of rare earths, *J. Less Common Metals* **127**, 373-378.
11. Chopra D, Babb H, Bhalla R. (1976) Appearance potential study of the 4f states of holmium, *Phys. Rev.* **B14**, 5231-5236.
12. Chopra DR, Chung HK. (1982) Soft X-ray appearance potential spectra of Ho and Ho/Ni alloy, *Appl. Surf. Sci.* **11/12**, 390-399.
13. Chopra DR, Hatwar TK. (1984) Soft X-ray appearance potential spectroscopy studies of DyFe<sub>2</sub> and ErFe<sub>2</sub> intermetallics, *Surf. Sci.* **140**, 216-226.
14. Chopra D, Martin G. (1982) Study of M<sub>4,5</sub>-level soft X-ray appearance potential spectra of selected rare earths, in: *The Rare Earths in Modern Science and Technology*, GJ McCarthy, HB Silber, JJ Rhyne (eds), Plenum, New York, Vol. 3, 131-134.
15. Chopra D, Martin G, Naraghi H, Martinez L. (1981) Soft x-ray appearance potential studies of <sup>59</sup>Pr, <sup>65</sup>Tb, <sup>67</sup>Ho, and <sup>68</sup>Er, *J. Vac. Sci. Technol.* **18**, 44-48.
16. Chourasia AR, Chafekar VD, Deshpande SD, Mande C. (1985) EXAFS study of intermetallics of the type RGe<sub>2</sub> (R = La, Ce, Pr, Nd, Sm, Gd, Tb, Dy, Ho, Er and Y) Part I: Determination of Ge-Ge distances, *Pramana* **24**, 787-795.
17. Crecelius G, Wertheim GK, Buchanan DNE. (1978) Core-hole screening in lanthanide metals, *Phys. Rev.* **B18**, 6519-6524.
18. Dev B, Brinkman H. (1970) L<sub>α</sub> radiation from cobalt, nickel and copper crystal surfaces. Determination of electron binding energies of surface atoms, *Ned. Tijdschr. Vacuum techn.* **8**, 176-184.
19. Dose V, Drube R, Hartl A. (1986) Empty electronic states in solid and liquid nickel, *Solid State Commun.* **57**, 273-275.
20. Dose V, Fauster T. (1979) Deconvolution of appearance potential spectra. II., *Appl. Phys.* **20**, 299-303.
21. Dose V, Fauster Th, Gossman HJ. (1981) The inversion of autoconvolution integrals, *J. Comp. Phys.* **41**, 34-50.
22. Dose V, Fauster Th, Scheidt H. (1981) Isochromat and SXAPS studies of empty electronic states in chromium, iron and nickel, *J. Phys. F* **11**, 1801-1809.
23. Dose V, Haertl A. (1981) Soft X-ray appearance potential spectroscopy of metallic glasses, *Phys. Rev. Lett.* **47**, 132-134.
24. Dose V, Reusing G. (1983) Critical point energies from appearance potential spectra of cobalt, nickel and copper, *Solid State Commun.* **48**, 683-685.
25. Dose V, Reusing G, Guntherodt HJ. (1984) Appearance potential spectroscopy of CuZr and CuTi metallic glasses, *Solid State Commun.* **49**, 1081-1083.
26. Dose V, Scheidt H. (1979) Deconvolution of appearance potential spectra, *Appl. Phys.* **19**, 19-23.
27. Dose V, Scheidt H. (1981) Isochromat and SXAPS measurements on hafnium, tantalum, and tungsten, *Phys. Stat. Solidi* **103**, 247-252.
28. Drube W, Himpfel FJ, Ludeke R. (1987) Inverse photoemission from surface and interface states of III-V semiconductors, *J. Vac. Sci. Technol. B* **5**, 930-932.
29. Eckertova L, Pavluch J. (1984) A modification of the AEAPS method, *Czech. J. Phys. B* **34**, 622-634.
30. Einstein TL, denBoer ML, Morar JF, Park RL, Laramore GE. (1981) Oxidation states by extended appearance potential fine structure, *J. Vac. Sci. Technol.* **18**, 490-491.
31. Einstein TL, Roelofs LD, Park RL, Laramore GE. (1979) Recent Progress in extended appearance potential fine structure analysis, *Bull. Am. Phys. Soc.* **24**, 506.
32. Erickson NE, Powell CJ. (1984) Comparison of L<sub>3</sub>-shell excitation energies of 3d transition metals obtained by XPD, AEAPS, and EELS, *J. Vac. Sci. Technol.* **A2**, 840-841.
33. Ertl G, Wandelt K. (1972) Soft x-ray appearance potential spectra of Ni/Cu alloys, *Phys. Rev. Lett.* **29**, 218-220.
34. Ertl G, Wandelt K. (1974) A soft x-ray appearance potential spectroscopy study of the oxidation of nickel, *Z. Naturforsch.* **29a**, 768-772.
35. Esteva JM, Karnatak RC, Fuggle JC, Sawatzky GA. (1983) Selection rules and multiple effects in comparison of x-ray absorption and photoemission peak energies, *Phys. Rev. Lett.* **50**, 910-913.
36. Fuggle JC, Campagna M, Zolnierrek Z, Lasser R, Plateau A. (1980) Observation of a relationship between core-level line shapes in photoelectron spectroscopy and the localization of screening

- orbitals, Phys. Rev. Lett. 45, 1597-1600.
37. Fukuda Y, Elam WT, Park RL. (1977) Absolute  $2p_{3/2}$  core binding energies and work functions of 3d transition-metal surfaces, Phys. Rev. B16, 3322-3329.
38. Gadzuk JW, Sunjic M. (1975) Excitation energy dependence of core-level x-ray-photoemission spectra line shapes in metals, Phys. Rev. B12, 524-530.
39. Gerlach RL, Houston JE, Park RL. (1970) Ionisation spectroscopy of surfaces, Appl. Phys. Lett. 16, 179-181.
40. Grolemond DL, Chopra D. (1983) Auger electron appearance potential spectrum of Ni, IEEE Transactions Nucl. Sci. NS-30, 934-936.
41. Harte WE, Szczechpanek PS. (1978) Soft X-ray appearance potential spectra of the rare earths, Jpn. J. Appl. Phys. 17-2 [Suppl.], 305-307.
42. Harte WE, Szczechpanek PS, Leyendecker AJ. (1983) Soft X-ray appearance potential spectroscopy of the lanthanide rare earths, J. Less Common Metals 93, 189-200.
43. Hatwar TK, Chopra DR. (1985) Electronic structure of La-Ni intermetallics: A soft X-ray appearance potential study, J. Elect. Spec. Rel. Phenom. 35, 77-85.
44. Hatwar TK, Chopra DR. (1985) Soft x-ray appearance potential spectroscopic study of rare earth-nickel intermetallics, Lanthanide Actinide Res. 1, 135-142.
45. Hillebrecht FU, Fuggle JC, Bennett PA, Zolnierok Z, Freiburg Ch. (1983) Electronic structure of Ni and Pd alloys. II. X-ray photoelectron core-level spectra, Phys. Rev. B27, 2179-2193.
46. Himpfel FJ, Fauster Th. (1984) Probing valence states with photoemission and inverse photoemission, J. Vac. Sci. Technol. A 2, 815-821.
47. Houston JE, Park RL. (1972) Difference in the Cr  $L_3/L_2$  intensity ratio measured by soft-x-ray and auger-electron appearance potential spectroscopy, Phys. Rev. B5, 3808-3809.
48. Hua ZY, Zhuge J, Fan CS, Chen HX, Pan XL, Huang JL. (1980) Soft x-ray appearance potential spectroscopy study of pure rare-earth metals with a sealed-off analyzer tube, J. Vac. Sci. Technol. 17, 211-213.
49. Kirschner J, Losch W. (1977) Comparison of Auger electron spectroscopy, Auger electron appearance-potential spectroscopy and disappearance potential spectroscopy in a cylindrical-mirror-analyzer system, J. Vac. Sci. Technol. 14, 1173-1179.
50. Kirschner J, Staib P. (1975) Disappearance potential spectroscopy, Appl. Phys. 6, 99-109.
51. Konishi R, Kinoshita M, Kato S. (1982) Low energy electron contributions to Auger electron appearance potential spectrum of carbon, Jpn. J. Appl. Phys. 21, 204-205.
52. Konishi R, Miyada Y, Sasakura H. (1985) Observation of sorption of  $O_2$  and  $N_2$  on Ti thin film by DAPS, AEAPS, AES and electrical resistance methods, Jpn. J. Appl. Phys. 24, 923-927.
53. Konishi R, Tanigawa H, Sasakura H. (1986) Extended appearance potential fine structure analysis of chromium, Jpn. J. Appl. Phys. 25, 1616-1617.
54. Lang JK, Baer Y. (1979) Bremsstrahlung isochromat spectroscopy using modified XPS apparatus, Rev. Sci. Instrum. 50, 221-226.
55. Lang JK, Baer Y, Cox PA. (1981) Study of the 4f and valence band density of states in rare earth metals: II. Experiment and results, J. Phys. F 11, 121-138.
56. Laramore GE. (1978) Geometrical information in soft-x-ray appearance potential spectroscopy and Auger electron appearance potential spectroscopy, Phys. Rev. B18, 5254-5264.
57. Laramore GE. (1979) The use of fourier transforms for analyzing the extended fine structure above appearance potential thresholds, Surf. Sci. 81, 43-56.
58. Laramore GE, Einstein TL, Roelofs LD, Park RL. (1980) Effect of the central atom potential on the extended fine structure above appearance potential thresholds, Phys. Rev. B21, 2108-2121.
59. Lee PA, Citrin PH, Eisenberger P, Kincaid BM. (1981) Extended x-ray absorption fine structure--its strengths and limitations as a standard tool, Rev. Mod. Phys. 53, 769-806.
60. Lee RN. (1977) Instrumental sensitivity in soft x-ray appearance potential spectroscopy, Rev. Sci. Instrum. 48, 1603-1609.
61. Ludeke R, Straub D, Himpfel FJ, Landgren G. (1986) Metal-derived band gap states: Ti on GaAs (110), J. Vac. Sci. Technol. A 4, 874-878.
62. Malik SK, Arlinghaus FJ, Wallace WE. (1982) Calculation of the spin-polarized energy-band structure of  $LaNi_5$  and  $GdNi_5$ , Phys. Rev. B25, 6488-6491.
63. Mehl MJ, Einstein TL, Bryant GW. (1984) Pseudodipole selection rules for extended fine structure in APS: Calculations and applications, J. Vac. Sci. Technol. A2, 862-863.
64. Morar JF, Park RL. (1983) Extended-fine-structure analysis of oxygen on titanium, J. Vac. Sci. Technol. A1, 1043-1046.
65. Nagel DJ. (1973) X-ray probes of vacant energy bands, in: Band Structure Spectroscopy of Metals and Alloys, DJ Fabian, LM Watson (eds), Academic, New York, 457-489.
66. Nilsson PO, Kanski J. (1972) The

## Appearance Potential Spectroscopy

- appearance potential spectrum of aluminum, Phys. Lett. A 41, 217-218.
67. Nilsson PO, Kanski J. (1973) Appearance potential spectroscopy of simple metals, Surf. Sci. 37, 700-707.
68. Nyberg C. (1975) The reaction of oxygen with Ti, Cr, Fe and Ni studied by appearance potential spectroscopy, Surf. Sci. 52, 1-9.
69. Nyberg C. (1979) Soft X-ray appearance potential spectroscopy of C, N and O adsorbed on Cr, Mo and W, Surf. Sci. 82, 165-176.
70. Osterwalder J. (1985) On the electronic structure of the light rare earth hydrides, Z. Phys. B 61, 113-128.
71. Palmberg PW. (1973) Quantitative analysis of solid surfaces by Auger electron spectroscopy, Anal. Chem. 45, 549A-556A.
72. Park RL. (1975) Recent developments in appearance potential spectroscopy, Surf. Sci. 48, 80-98.
73. Park RL. (1979) Recent progress in surface analysis, Surf. Sci. 86, 504-515.
74. Park RL, denBoer ML, Fukuda Y. (1974) Appearance potential spectra from the secondary electron yield, in: Proc. 6th Czech. Conf. Electr. Vac. Phys., Bratislava, 4, 53-59.
75. Park RL, Houston JE. (1971) Appearance potential spectroscopy on an austere budget, Surf. Sci. 26, 664-666.
76. Park RL, Houston JE. (1972) L-shell soft X-ray appearance potential spectra of the 3d transition metals, Phys. Rev. B 6, 1073-1081.
77. Park RL, Houston JE. (1974) Soft X-ray appearance potential spectroscopy, J. Vac. Sci. Technol. 11, 1-18.
78. Park RL, Houston JE, Schreiner DG. (1970) A soft x-ray appearance potential spectrometer for the analysis of solid surfaces, Rev. Sci. Instrum. 41, 1810-1812.
79. Pavluch J, Eckertova L. (1985) A new appearance potential spectrometer, Czech. J. Phys. B 35, 630-642.
80. Pendry JB. (1980) New probe for unoccupied bands at surfaces, Phys. Rev. Lett. 45, 1356-1358.
81. Richardson OW, Bazzoni CB. (1921) The excitation of soft characteristic x-rays, Philos. Mag. 42, 1015-1019.
82. Ritchie RH, Tung CJ, Anderson VE, Ashley JC. (1975) Electron slowing-down spectra in solids, Radiant Res. 64, 181-204.
83. Schlapbach L, Scherrer HR. (1982) XPS core level and valence band spectra of LaH<sub>3</sub>, Solid State Commun. 41, 893-897.
84. Schulz SW, Schleidcher KT, Ruck DM, Chun HU. (1984) Derivation of the density of unoccupied states in polycrystalline ferromagnetic Fe, Co, and Ni from highly resolved appearance potential spectra, J. Vac. Sci. Technol. A2, 822-825.
85. Shinoda G, Suzuki T, Kato S. (1954) Two types of band emission curves of copper in the soft x-ray region, Phys. Rev. 95, 840-841.
86. Shulakov AS, Zimkina TM, Stepanov AP. (1985) Nature of the lanthanum appearance potentials N<sub>4,5</sub> spectrum fine structure, Sov. Phys. Solid State 27, 65-68.
87. Smith RJ, Piacentini M, Wolf JL, Lynch DW. (1976) Soft X-ray appearance potential spectra of La and Ce from 0 to 1400 eV, Phys. Rev. B14, 3419-3431.
88. Snow EC, Waber JT. (1969) The APW energy bands for the body centered and face centered cubic modifications of the 3d transition metals, Acta Met. 17, 623-635.
89. Speier W, Fuggle JC, Zeller R, Ackermann B, Szot K, Hillebrecht FU, Campagna M. (1984) Bremsstrahlung isochromat spectra and density-of-states calculations for the 3d and 4d transition metals, Phys. Rev. B30, 6921-6930.
90. Stern EA. (1974) Theory of the extended x-ray absorption fine structure, Phys. Rev. B10, 3027-3037.
91. Stern EA, Sayers DE, Lytle FW. (1975) Extended x-ray-absorption fine-structure technique. III. Determination of Physical parameters, Phys. Rev. B11, 4836-4846.
92. Stohr J, Denley D, Perfetti P. (1978) Surface extended x-ray absorption fine structure in the soft-x-ray region: Study of an oxidized Al surface, Phys. Rev. B18, 4132-4135.
93. Stohr J, Johansson LI, Brennan S, Hecht M, Miller JN. (1980) Surface extended-x-ray-absorption-fine-structure study of oxygen interaction with Al (111) surfaces, Phys. Rev. B22, 4052-4065.
94. Teo BK, Lee PA. (1979) Ab initio calculations of amplitude and phase functions for extended x-ray absorption fine structure spectroscopy, J. Am. Chem. Soc. 101, 2815-2832.
95. Tong SY. (1984) Exploring surface structure, Physics Today 37, no.8, 50-59.
96. Tracy JC. (1972) Appearance potential spectroscopy, J. Appl. Phys. 43, 4164-4171.
97. Turtle RR, Liefeld RJ. (1973) Densities of unfilled one-electron levels in the elements vanadium and iron through zinc by means of x-ray continuum isochromats, Phys. Rev. B7, 3411-3419.
98. Wandelt K, Ertl G. (1976) Electron spectroscopic studies of the oxidation of Fe/Ni alloys, Surf. Sci. 55, 403-412.
99. Webb C, Williams PM. (1974) Comparison of binding energies determined by appearance potential spectroscopy and X-ray photoemission spectroscopy, Phys. Rev. Lett. 33, 824-827.
100. Wendin G. (1974) Localized excita-

tions in appearance potential spectra in barium, in : Proceedings of the International Conference on Vacuum-Ultraviolet Radiation in Physics, Hamburg, Vieweg-Pergamon, Braunschweig, 252-254.  
101. Wendin G, Nuroh K. (1977) Bremsstrahlung resonances and appearance potential spectroscopy near the 3d thresholds in metallic Ba, La and Ce, Phys. Rev. Lett. 39, 48-51.

Discussion with Reviewers

T.J. Shaffner: Could APS be used in conjunction with inert gas sputter etching for depth profiling? Would this alter the density of unoccupied states beyond recognition?

Authors: No experimental data are available for the sputter depth profiling of materials by APS.

T.J. Shaffner: Would you anticipate any advantages of APS over other surface sensitive techniques, such as XPS and AES, for the analysis of the new high Tc YBa<sub>2</sub>Cu<sub>3</sub>O<sub>7-x</sub> superconducting materials?

Authors: Again, no experimental data are available for superconducting materials. The advantages of APS over XPS and AES have been pointed out with suitable examples in this paper.